# THE DEPENDENCE OF IMPULSE PROPAGATION SPEED ON FIRING FREQUENCY, DISPERSION, FOR THE HODGKIN-HUXLEY MODEL

ROBERT N. MILLER AND JOHN RINZEL, *Mathematical Research Branch, National Institute of Arthritis, Metabolism and Digestive Diseases, National Institutes of Health, Bethesda, Maryland 20205*

ABSTRACT Propagation speed of an impulse is influenced by previous activity. A pulse following its predecessor too closely may travel more slowly than a solitary pulse. In contrast, for some range of interspike intervals, a pulse may travel faster than normal because of a possible superexcitable phase of its predecessor's wake. Thus, in general, pulse speeds and interspike intervals will not remain constant during propagation. We consider these issues for the Hodgkin-Huxley cable equations. First, the relation between speed and frequency or interspike interval, the dispersion relation, is computed for particular solutions, steadily propagating periodic wave trains. For each frequency, $\omega$, below some maximum frequency, $\omega_{max}$, we find two such solutions, one fast and one slow. The latter are likely unstable as a computational example illustrates. The solitary pulse is obtained in the limit as $\omega$ tends to zero. At high frequency, speed drops significantly below the solitary pulse speed; for 6.3°C, the drop at $\omega_{max}$ is >60%. For an intermediate range of frequencies, supernormal speeds are found and these are correlated with oscillatory swings in sub- and superexcitability in the return to rest of an impulse. Qualitative consequences of the dispersion relation are illustrated with several different computed pulse train responses of the full cable equations for repetitively applied current pulses. Moreover, changes in pulse speed and interspike interval during propagation are predicted quantitatively by a simple kinematic approximation which applies the dispersion relation, instantaneously, to individual pulses. One example shows how interspike time intervals can be distorted during propagation from a ratio of 2:1 at input to 6:5 at a distance of 6.5 cm.

## 1. INTRODUCTION

During impulse propagation in nerve, several factors (e.g., nonuniform membrane properties, nonuniform ionic environment, or geometrical factors such as branching or changes in diameter) can influence spike timing and conduction time. However, even in cases of uniform geometry, uniform membrane properties and uniform ionic environment, not all pulses will travel at the same speed. In particular, the speed of pulses in a train depends upon the time interval between adjacent pulses. A pulse following too closely behind its predecessor may travel at reduced speed because of the recovery wake into which it advances. For some fibers, on the other hand, certain ranges of interspike intervals actually lead to supernormal conduction velocities (see, for example, reference 8). Because propagation speed depends on

---

Dr. Miller's present address is the Division of Applied Sciences, Harvard University, Cambridge, Massachusetts 02138.

interspike interval, i.e., because of dispersion, pulse speeds and hence interspike intervals may change during propagation so that, in general, precise timing of individual pulses may not be maintained. In this paper we focus on dispersive aspects of impulse propagation and present explicit theoretical results for the Hodgkin-Huxley (HH) model (20). A useful quantitative characterization of dispersive properties is the relation between propagation speed and frequency for a periodic train of uniformly spaced pulses traveling with fixed speed. We have calculated (see section 2 below) such periodic traveling wave solutions and their dispersion relation for the HH equations; strong temperature dependence is indicated by results for three different temperatures. We observe in this relation a considerable decrease in speed at higher frequencies. At higher temperatures, a midrange of frequencies appears with supernormal speeds and amplitudes. The dispersion relation also predicts the maximum firing frequency, $\omega_{max}$, for the model fiber. In section 3 we present numerical solutions for the full cable equations without the assumption of a steadily traveling wave train. These results illustrate that speeds and interspike intervals can change significantly during propagation in response to repetitive current stimulation delivered at a single point. They also demonstrate that the cable fails to follow in a one-to-one fashion (i.e., one propagated nerve impulse per each stimulus pulse) for a stimulus frequency greater than $\omega_{max}$. In one example we find that pulses in a train alternate between sub- and supernormal conduction velocities.

Finally, in section 4, we derive a simple approximate procedure to predict changes of *individual* interspike intervals during propagation. In this procedure, only the dispersion relation along with observations at a single location downstream from the stimulus are used. The full cable equations need not be solved to apply the procedure. Approximate results compare well with the stimulus-response simulations of section 3.

Few experimental studies have used periodic stimulation to investigate dispersion. In one such case, Arshavskii et al. (2) used electronics to simulate a ring of frog or worm axon by feeding a pulse in one end of the axon when a pulse was detected at the other end. Using this experimental setup, they observed the speed of the pulses on the ring to decrease with decreasing time interval. They also found that a fiber of a given length could only sustain a limited number of pulses (in their case no more than two pulses could be introduced into the axon of an earthworm 10–15 cm long). This is consistent with the notion of a minimum wavelength for pulse trains. Several investigators have reported variations in conduction speed (i.e., usually conduction time measured between electrodes at two locations) of a pulse which is initiated at different time intervals following a preceding pulse or burst. These reports for frog (16, 38, 3), squid (8, 37), earthworm (3), aplysia (17), and mammalian CNS (14, 28, 46, 47) usually acknowledge the slower speed of a pulse which follows its predecessor too closely but in many cases have emphasized the phenomenon of supernormal or facilitated conduction speed. In such cases it is generally found that for interspike intervals greater than a certain minimum the second pulse of a pair actually travels faster than the first. As a function of increasing interval the speed of the second pulse reaches a maximal value and then decreases to approach that of the first from above. Our calculated dispersion relation exhibits similar behavior.

Calculations performed by Ramon et al. (37) for the Hodgkin-Huxley cable equations compared favorably with their two pulse experiments on squid and illustrated changes in conduction speed, although the case of supernormal speed was not treated. Theoretical

arguments using reduced descriptions of propagation and/or qualitative features of a presumed dispersion relation have been correlated with two pulse experiments (25, 8, 44, 16, 2). In those studies the existence of a supernormal range and a nonmonotone dispersion relation for long wavelength and temporal period was found to be the crucially important factor in the phenomenon of pulses locking into pairs or groups during propagation. Calculations by Karfunkel and Kahlert (25) for a model excitable chemical reaction in a one dimensional ring geometry demonstrated pulse locking explicitly. Kocsis et al. (28) offer experimental evidence for locking (or entrainment, in their terminology) of pulses propagating along axons of visual cortical efferent neurons in the rabbit. Some of our results will be discussed in the context of pulse locking.

Theoretical studies of nerve conduction equations which restrict themselves to the special assumption of traveling wave solutions have been pursued both analytically and numerically. Results have been obtained for the HH model, or versions of it with exaggerated time scale differences between slower and faster processes, and also for equations of the FitzHugh-Nagumo (FHN) type (11, 34, 6). Hodgkin and Huxley (20) computed a solitary pulse solution and found the predicted speed to agree well with the experimentally observed speed. Huxley (22) computed a different pulse shaped solution with much smaller speed and amplitude and conjectured that it was unstable since pulses of that form were not observed. Other investigators, including Cooley and Dodge (7), FitzHugh and Antosiewicz (13), Evans and Feroe (9), and Hassard[1] have also computed solitary pulse solutions. Evans and Feroe (9) have shown that the fast pulse is stable and the slow one is not. Periodic traveling wave solutions and the dispersion relations associated with them have not previously been computed for the Hodgkin-Huxley equations, although Carpenter (4) has used singular perturbation methods and a geometrical technique to show the existence of periodic solutions and solitary pulses (presumably the stable ones) under the assumption that the kinetics of the sodium activation parameter $m$ are very much faster than those of the sodium inactivation $h$ or the potassium activation $n$. Numerical solutions of Stein (45) and Cooley and Dodge (7) for the full HH cable equations under constant current stimulation resemble periodic traveling waves downstream from the stimulus and after sufficient time.

Existence proofs (4, 19), singular perturbation constructions (6), stability results (29), and numerical calculations (11, 40) have been provided for solitary pulse and periodic traveling wave solutions to the FHN equations. Rinzel and Keller (41) studied a piecewise linear FHN type model (31) for which the traveling wave equation is solvable analytically. For a range of parameter values they determined the periodic traveling waves as a one-parameter family described by the dispersion relation, i.e., speed vs. frequency. They found typically that periodic solutions to the traveling wave problem do not exist for frequencies above some maximum frequency $\omega_{max}$. For frequencies $\omega < \omega_{max}$ two solutions were found, one fast and one slow; the solitary pulse solutions are obtained in the limit as $\omega$ decreases to zero. They further demonstrated that the slow waves are unstable. Rinzel (39) showed that an exchange of stability occurs at $\omega_{max}$. Our findings[2] for the HH equations are qualitatively similar to those

[1]Hassard, B. D. Manuscript submitted for publication.

[2]Preliminary reports of some of the results presented here were given in 43 and 32.

of Rinzel and Keller (41). The computed dispersion relation is double branched so that there are two periodic traveling wave solutions, one fast and one slow, for each frequency less than $\omega_{max}$. The slow family of periodic wavetrains has not been observed in nature and is thought to be unstable. We show a computational example that is consistent with this hypothesis.

The traveling wave problem for nerve model equations may have solutions that are more intricate than the solitary pulse and the periodic waves. Such possibilities as wavetrains of finite length and periodic bursts of pulses have been investigated by Carpenter (5) and Feroe (10). We did not compute such solutions in this study.

## 2. PERIODIC TRAVELING WAVE SOLUTIONS

### *The Hodgkin-Huxley Model*

The Hodgkin-Huxley (20) model of a nerve fiber of uniform diameter is given by the following system of partial differential equations:

$$\begin{aligned}(a/2R)V_{xx} &= CV_t + I_i(V, m, h, n)\\ m_t &= \phi(\text{Temp})(m_\infty(V) - m)/\tau_m(V)\\ h_t &= \phi(\text{Temp})(h_\infty(V) - h)/\tau_h(V)\\ n_t &= \phi(\text{Temp})(n_\infty(V) - n)/\tau_n(V),\end{aligned} \tag{1}$$

where the ionic current density is defined by $I_i(V, m, h, n) = \bar{g}_{Na}m^3h(V - V_{Na}) + \bar{g}_K n^4(V - V_K) + g_L(V - V_L)$. The temperature correction factor satisfies $\phi(\text{Temp}) = \exp[\ln 3 \cdot (\text{Temp} - 6.3°\text{C})/10°\text{C}]$.

$V$ here is the membrane potential, with depolarization considered to be the positive sense. The auxiliary variables $m$, $h$, and $n$ are dimensionless quantities which range between zero and one. They reflect the degree of sodium activation, sodium inactivation, and potassium activation, respectively. $m_\infty$, $\tau_m$, $h_\infty$, $\tau_h$, $n_\infty$, and $\tau_n$ are given functions of $V$. Their exact forms are complicated; these can be found in FitzHugh (11). Values of the constants are: $a$, fiber radius = 238 $\mu$m; $R$, specific core resistance = 35.4 $\Omega$·cm; $C$, membrane capacitance = 1 $\mu$F/cm$^2$; $\bar{g}_{Na}$, fully activated sodium conductance = 120m $\nu$/cm$^2$; $\bar{g}_K$, fully activated potassium conductance = 36m $\nu$/cm$^2$; $g_L$, leakage conductance = 0.3m $\nu$/cm$^2$; $V_{Na}$, sodium equilibrium potential = 115 mV; $V_K$, potassium equilibrium potential = $-12$ mV; $V_L$, leakage potential = 10.5989 mV. We have chosen these values for historical reasons. These were the original values used by Hodgkin and Huxley (20), and later by Cooley and Dodge (7) for their calculations. This choice of parameters makes our calculations directly comparable to those cited above without a change of scale.

It is important to be aware of scaling considerations (12, 23). One might, for example, introduce a length constant $\lambda = (a/2R\,G_0)^{1/2}$, where $G_0 = \bar{g}_{Na}\,m_\infty^3(0)\,h_\infty(0) + \bar{g}_K\,n_\infty^4(0) + g_L$. Those of our results which depend on a distance scale could be expressed relative to dimensionless distance $y = x/\lambda$ and hence could be applied to cases with different values for the passive parameters $a$ and $R$. We remind the reader that we are not free to change the time scale as well without changing the characteristics of the membrane model. If one were to nondimensionalize time, say $s = t/\tau$ where $\tau = C/G_0$, the value of $\tau$ would influence the rates $m_t$, $h_t$, and $n_t$. Therefore, our results are not applicable, for example, for arbitrary values of $C$.

We introduce the traveling coordinate $z = kx + \omega t$, and seek a periodic solution of the form:

$$\begin{aligned} V(x, t) &= u(z) \\ m(x, t) &= p_1(z) \\ h(x, t) &= p_2(z) \\ n(x, t) &= p_3(z). \end{aligned} \tag{2}$$

The period is fixed at $2\pi$ so that

$$u(z + 2\pi) = u(z); p_j(z + 2\pi) = p_j(z), j = 1, 2, 3. \tag{3}$$

In this coordinate system, $k$ is the wave number (a spatial frequency) and $\omega$ is the temporal angular frequency. These quantities are related to the wavelength $P$ in centimeters and the period $T$ in milliseconds by

$$\begin{aligned} k &= 2\pi/P \\ \omega &= 2\pi/T, \end{aligned} \tag{4}$$

and the propagation speed $\theta = \omega/k$.

Only a few special sets of boundary conditions for Eq. 1 can be fulfilled by a solution of the form, Eq. 2. For example, an infinite uniform fiber or a uniform ring of appropriate length could support a solution of this form. However, it seems intuitively reasonable that such traveling wave solutions could provide a useful approximate description of impulse propagation under certain conditions, e.g., sufficiently far from the point of stimulation in a long uniform fiber. The original computation of Hodgkin and Huxley (20) for the single-pulse solution is equivalent to a limiting case of Eq. 2 in which $k$ and $\omega$ approach zero with $\omega/k = \theta$, the speed of the single pulse. This showed good agreement with experiment. The results of our more general calculations shown in section 3 below also indicate that the traveling wave assumption is reasonable in some more general settings. Substitution of functions of the form given in Eq. 2 into the partial differential Eq. 1 yields the following equations which a traveling wave solution to Eq. 1 must satisfy:

$$\begin{aligned} k^2u'' &= \omega u' + I_i(u, p_1, p_2, p_3) \\ \omega p_1' &= \phi(\text{Temp})(m_\infty(u) - p_1)/\tau_m(u) \\ \omega p_2' &= \phi(\text{Temp})(h_\infty(u) - p_2)/\tau_h(u) \\ \omega p_3' &= \phi(\text{Temp})(n_\infty(u) - p_3)/\tau_n(u). \end{aligned} \tag{5}$$

If suffices to consider only one interval $0 \leq t \leq 2\pi$ where the solution satisfies the boundary conditions given in Eq. 3 with $z = 0$.

For each frequency $\omega$ at which the model exhibits steady repetitive firing, we expect a solution to Eq. 5 with appropriate wavelength or pulse spacing $P$ and speed $\omega/k$. Conversely, we could fix $k$ (and thus $P$) and seek a solution with appropriate temporal frequency $\omega$, but we cannot, in general, fix $k$ and $\omega$ arbitrarily and expect to find a solution.

*Waves and the Dispersion Relation*

Eq. 5 was solved numerically for the periodic wave and either $k$ or $\omega$ by a method described in the Appendix. Our results indicate the highly dispersive character of these waves. In many

applications the term "dispersion relation" is reserved for the relation between $\omega$ and $k$. Here we will also use it to refer to other parameterizations of this relation, e.g., $\theta$ vs. $\omega$ (Fig. 1) or $\theta$ vs. $P$ (Fig. 2). Each point on such graphs represents a computed traveling wave solution. The dashed lines correspond to the speeds $\theta_f$, $\theta_s$ of the fast and slow solitary pulses, respectively, at these three temperatures. Previous investigators (7, 9, 20, 22, and a referee) computed one or more of the speeds $\theta_f$, $\theta_s$ for 6.3° and 18.5°C, and $\theta_f$ for 26°C, by the shooting method for a uniformly propagated pulse. Values for $\theta_f$ are given in Table I. Since a value for $\theta_s$ for 26°C was not found in the literature we estimated it from the limit of low frequency slow wave trains. As seen in Figs. 1 and 2, our speeds, in the limit of low frequency or long wavelength wave trains, are in good agreement with the solitary pulse speeds. The reader should recall here that changes in fiber diameter have the effect of a change of scale, as was discussed above. Thus the shapes of the curves will not be affected by such changes.

From the curves of Fig. 1 we can read off the maximum firing frequency $\omega_{max}$ for a propagated train (see Table I) and observe that $\omega_{max}$ increases with temperature. This is consistent with the general trend of increasing frequency with temperature for space- and current-clamped membrane (42). Increased temperature has the effect of speeding up the recovery processes, thus decreasing the refractory period and allowing shorter time intervals between spikes. Temperature significantly affects the dependence of propagation speed on frequency (Fig. 1). Of the three temperatures shown, dispersion is greatest at 6.3°C; the speed falls from 12.3 m/s for the solitary pulse to a speed of 4.6 m/s at the maximum frequency of 147 Hz. At higher temperatures less dispersion appears, i.e., the speed at maximum frequency is closer to the speed of the solitary pulse (see Table I). For 6.3°C, the falling phase of the

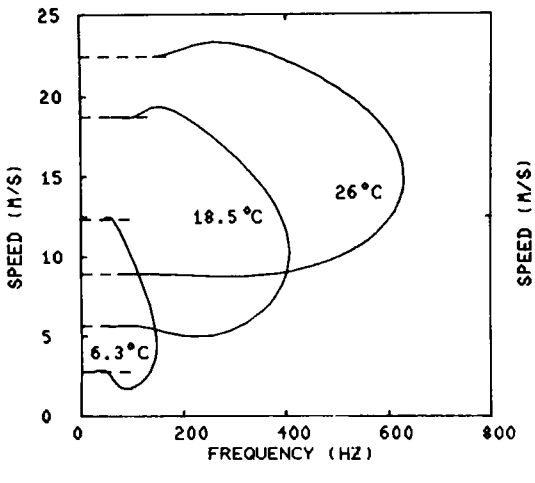


FIGURE 1

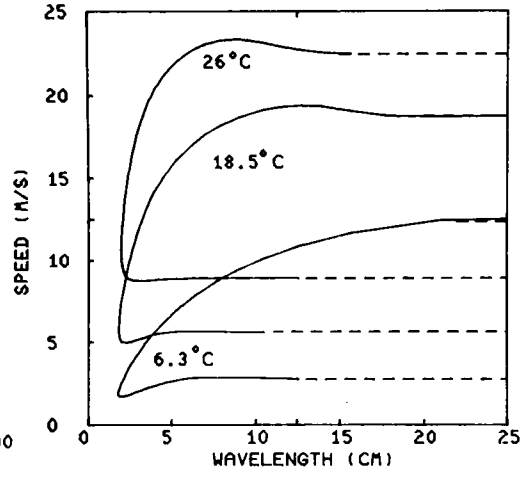


FIGURE 2

FIGURE 1 Computed dispersion relations, conduction speed vs. firing frequency, for periodic traveling wave solutions to the Hodgkin-Huxley equations for three temperatures. Speeds of the fast and slow solitary pulses (shown dashed) represent the limiting speeds of the periodic waves as the frequency approaches zero. The phenomenon of supernormal conduction speed over the low to mid-frequency range is clearly illustrated. M/S, meter/second; HZ, hertz.

FIGURE 2 The relation between conduction speed and wavelength for traveling wave solutions to the Hodgkin-Huxley equations. CM, centimeter.

TABLE I
SPEED/FREQUENCY DATA FOR PERIODIC WAVE TRAINS

| Temperature | $\omega^*_{max}$ | $\theta(\omega_{max})^*$ | $\theta_f$ | $\theta_{max}$ | $\omega(\theta_{max})$ | $\omega(\theta_f)$ |
|---|---|---|---|---|---|---|
| 6.3° | 147 | 4.62 | 12.31 | 12.59 | 50.0 | 62.6 |
| 18.5° | 407 | 10.23 | 18.73‡ | 19.41 | 152 | 208 |
| 26.0° | 631 | 14.67 | 22.47 | 23.31 | 264 | 388 |

*Frequencies given in Hz; propagation speed given in m/s.
‡18.74 in references 6, 12.

curve is very steep over a smaller frequency range. For the higher temperatures, the drop in speed occurs over a broader but much higher frequency range so that velocity sensitivity is restricted to a narrow range of interspike intervals and velocity shows relatively little sensitivity to frequency over a considerable low and intermediate frequency range.

The dispersion curves of speed vs. wavelength are shown in Fig. 2. At 6.3°C only wavetrains with very long wavelengths travel at speeds comparable to that of the fast solitary pulse, while the corresponding upper branches of the curves for 18.5° and 26°C are fairly flat. The wavelength data of Fig. 2 explicitly illustrate the spatial scales relevant for HH wave trains. For application to the large-diameter, rapidly conducting, squid axon one would not expect to see more than one pulse simultaneously on a fiber of physiological length (except for very high frequency stimulation). In this case, one might best view dispersive interactions from a temporal rather than spatial viewpoint. If one scales these curves for smaller diameter fibers then the spatial interpretation takes on greater importance. The speed vs. wavelength relation has further and direct applicability to propagation phenomena in the ring geometry as considered by Arshavskii et al. (2) for nerve impulses, by Karfunkel and Kahlert (25) for chemical waves, and by Rinzel (43) for kinematic approximations to pulse trajectories. Our predicted minimum wavelength represents a lower bound on the length of a ring which can sustain a steadily circulating pulse. The minimum ring length may in fact be larger because the minimum wavelength pulses may be unstable. Indeed, minimum wavelength of Fig. 2 is realized on the slow, and conjectured unstable, branch of the corresponding dispersion curve of Fig. 1. Yet we know of no theoretical justification for the belief that minimum stable wavelength for ring propagation corresponds to maximum frequency. Moreover, physical justification for this belief is not apparent since the geometry and boundary conditions for the phenomenon of minimum ring length differ from that of maximum frequency for periodic stimulation at the end of a long axon. Finally, we note that because the minimum wavelength pulses may be unstable there may be no direct biophysical interpretation of the relative temperature independence for the minimum wavelength.

A noticeable feature of the dispersion curves is the increase in speed over $\theta_f$, the speed of the solitary pulse, for a certain range of intermediate frequencies. This supernormal speed hump is small for 6.3°C but somewhat more pronounced at higher temperature. The frequency at which $\theta = \max_{\omega} \theta \equiv \theta_{max}$ and the highest nonzero frequency for which $\theta = \theta_f$, as well as the value of $\theta_{max}$, are presented in Table I. As noted in our introduction, supernormal conduction velocity has been observed for two pulse experiments in several preparations, including squid (cf. section 1 for references), as well as in theoretical simulations of two pulse experiments (16, 18). The phenomenon has in some cases been associated through experimental studies

(28, 38) and qualitative theoretical arguments (44) with an oscillatory phase of recovery during which the fiber is thought to be more excitable than at rest. This oscillatory recovery was observed experimentally by Mauro et al. (30) for space clamped squid axon membrane (although for a different species from the one used by Hodgkin and Huxley). They then explored the predictions of the Hodgkin-Huxley model for the subthreshold oscillations and found them in qualitative agreement with experiment (30). We shall discuss the relation between this oscillatory recovery phase and supernormal conduction in section 5 below.

Fig. 3 shows peak-to-peak amplitude of the membrane potential profile (i.e., max $V$ − min $V$) as a function of frequency for the computed wavetrains. The overall decrease in amplitude with increasing temperature is consistent with the increased rate of change of the recovery variables, i.e., $h$ decreases and $n$ increases significantly during the upstroke. Presumably as the temperature increases, these amplitude curves become narrower, the amplitudes of the slow low frequency wavetrains approaching those of the corresponding fast wavetrains until such impulse propagation fails entirely at 38°C (23). In a corresponding way, we expect (Figs. 1 and 2) the speeds of these wavetrains to coalesce. It is interesting to note that the peak amplitudes occur at some frequency strictly greater than zero. Like the phenomenon of maximum speed occurring at nonzero frequency, this is probably related to the fact that during some phases late in the recovery of the solitary pulse, the fiber is actually more excitable than it is at rest. A careful comparison of Fig. 3 with Fig. 1, however, will show that peak amplitude occurs at a somewhat higher frequency than peak speed.

Fig. 4 shows five selected temporal profiles of computed solutions to the periodic traveling

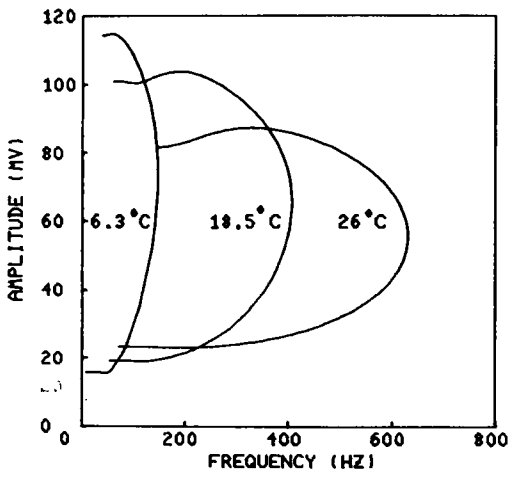


FIGURE 3

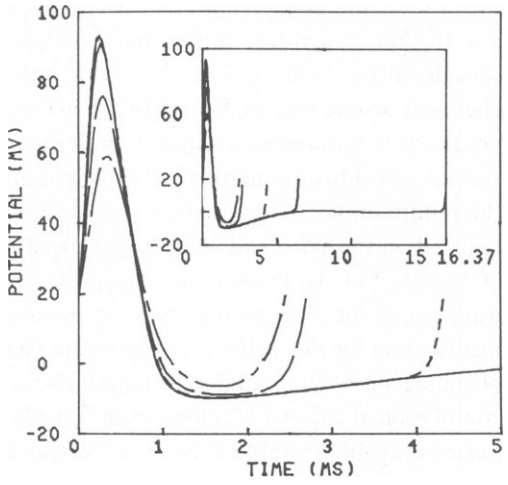


FIGURE 4

FIGURE 3 Peak to peak amplitude of membrane potential ($V_{max}$ − $V_{min}$) vs. frequency for periodic traveling wave solutions to the Hodgkin-Huxley equations. MV, millivolts; HZ, hertz.

FIGURE 4 Temporal profiles of traveling wave solutions to the Hodgkin-Huxley equations for five selected frequencies: 61, 154, 231, 370, and 407 Hz; temperature, 18.5°C. Note similar duration of upstroke, shoulder, and downstroke over this wide range of frequencies. Solid curve is actually two curves which coincide closely over the first 5 ms, being distinguishable only at the very peak of the upstroke. (Inset) similar to main figure, with time axis rescaled. Note the divergence of the two solid curves at ~7 ms. Note also that a slight overshoot is discernible in the recovery phase of the lowest frequency wave. MV, millivolt; MS, millisecond.

wave problem. These solutions for 18.5°C are from the upper branches of the curves in Figs. 1–3. The important feature of this figure and its inset is that all of the waves plotted here spend very nearly the same amount of time from spike upstroke through downstroke. The differences in time period in this range of frequencies appear to consist almost entirely of differences in duration of recovery. All of the waves (except those with the shortest time period) follow a common voltage time course most of the way through the recovery phase until the next upstroke.

This phenomenon is also apparent in Fig. 5, which shows the paths of several of our computed solutions projected on the *V-n* plane. As time progresses, the path of the specified solution is traversed in the counterclockwise direction. The rest point is shown as a cross (which in this graph is largely obscured by the 61-Hz solution). If the solitary pulse were shown in this diagram, its trajectory would begin and end at the rest point and it would be almost indistinguishable from the 61-Hz solution. In this representation, the recovery phase of the action potential is the nearly vertical segment on the left side of the picture along with the return to the vicinity of the singular point for the lower frequency wave. Thus we see convincingly that the wavetrains, except for the lowest period ones shown, follow a common recovery pathway through the phase space (evident in this *V-n* projection as well as other projections), leaving this pathway only at the time of the rapid upstroke of the next spike in the train.

The velocity of the wave train in such cases is determined by the recovery state, or equivalently the time duration spent on the common recovery pathway, at the point from which the next upstroke emerges. While it is anticipated that the recovery phase for lowest frequency spikes follows the solitary pulse pathway, here we find that this applies over a

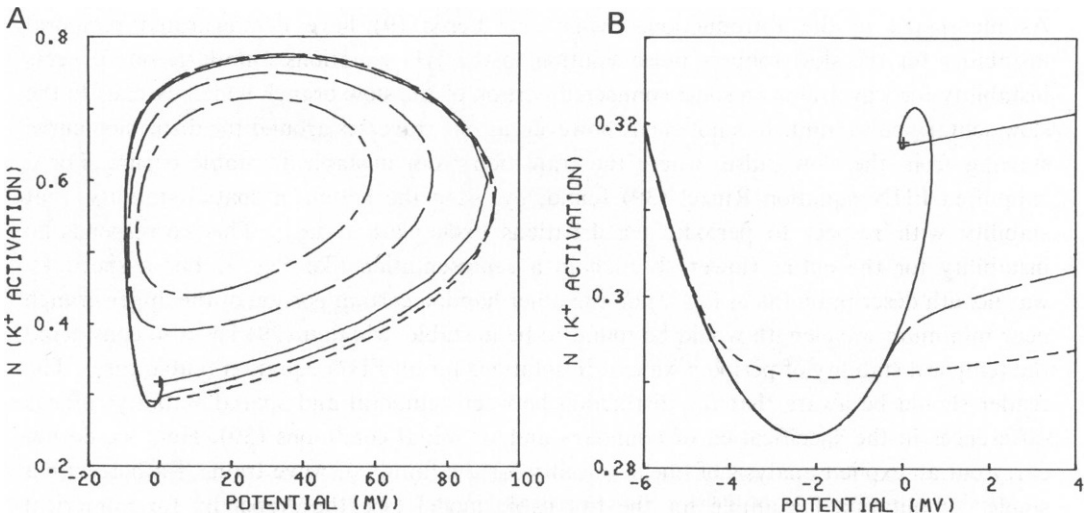


FIGURE 5 (*A*) Phase space trajectories of periodic traveling wave solutions of Fig. 4 projected on the *V-n* plane. The recovery phases are the nearly vertical segments at the left of the figure. Note that the three lowest frequency trajectories follow a nearly indistinguishable recovery path. (*B*) Detail of trajectories near the rest point. The undershoot of *n*, $K^+$ activation, is obvious here. In the phase during which the $K^+$ activation is less than its resting value the fiber may be more excitable than it is at rest, depending on the values of *m* and *h*. MV, millivolts.

considerable frequency range: $\omega \leq 250$ Hz for 18.5°C and $\omega \leq 100$ Hz for 6.3°C. For these ranges, the recovery state which follows a propagating spike can be described reasonably by a single parameter, time since downstroke or equivalently interspike interval, since spike width is fairly constant.

Let us now examine Fig. 5 more closely to gain insight into the increased amplitudes and conduction speeds of the low to mid frequency periodic waves over the solitary pulse. Observe for the lower frequency waves that there is an undershoot in $n$ at the end of the recovery, i.e., during some interval at the end of the recovery the potassium conductance is actually less activated than it is at rest. Similarly, although not shown here, the value of the sodium inactivation $h$ swings above its resting level. Fig. 5 *B* shows a magnification of the vicinity of the rest point from Fig. 5 *A*. Both the 154- and 231-Hz trajectories leave the common recovery path to begin their upstrokes at a point on the recovery path in which the potassium activation $n$ is below, and the sodium inactivation $h$ is above, its resting value, and thus the fiber may be more excitable than it is at rest. Both the solution for 231 and 154 Hz are larger in amplitude than the solitary pulse, but the 154-Hz solution travels faster than the solitary pulse while the 231-Hz solution travels more slowly. At higher temperatures the trajectory of the solitary pulse spirals into the rest point and it is not inconceivable that the graphs of amplitude vs. frequency and speed vs. frequency could be more intricate; for example, an oscillatory approach of $\theta$ to $\theta_f$ as $\omega$ tends to zero (see also section 5).

### *Computational Demonstration of Instability of a Slow Wave*

Motivated by Huxley's conjecture (22), we next address the hypothesis that certain slow waves are unstable as solutions to the partial differential (cable) Eq. 1. This consideration is important because only those solutions which are stable correspond to observable phenomena. As mentioned in the Introduction, Evans and Feroe (9) have demonstrated temporal instability for the slow solitary pulse solution to the HH equations. Similarly one expects instability for wavetrains on some connected portion of the slow branch which extends to the slow solitary pulse limit. It is not clear, however, as one traverses around the dispersion curve starting from the slow pulse, where the transition from unstable to stable occurs. For a simplified FHN equation Rinzel (39) found, by using the notion of spatial stability, that stability with respect to periodic perturbations exchanges at $\omega_{max}$. This corresponds to instability for the entire (lower) branch in a representation like Fig. 1. For a speed vs. wavelength description (as in Fig. 2) on the other hand, a certain portion of the upper branch near minimum wavelength would be found to be unstable. Maginu (29) has also considered the temporal stability of periodic wavetrain solutions for an FHN equation (cubic case). The reader should be aware that the distinction between temporal and spatial stability reflects differences in the specification of boundary and/or initial conditions (39). Here we do not carry out an explicit analysis of linear stability for the family of wave trains. Rather, with a single computational example for the full cable model (see the Appendix for numerical method), we illustrate how a slow small amplitude wave train, given as data, evolves into a fast large amplitude wave train under conditions most favorable to persistence of the slow periodic wave. For our model fiber ($0 \leq x \leq \ell$, $\ell = 10.0$ cm) we specify at $x = 0$ a potential whose time course is given by our computed slow wave train solution. This traveling wave solution is also

used as the initial condition. To motivate the boundary condition for $x = \ell$, assume that the solution is a wave traveling from left to right with speed $\theta$, then

$$V(x, t) = U(x - \theta t);$$

hence

$$V_t = -\theta V_x. \tag{6}$$

Eq. 6, which is referred to as an outgoing wave condition in many physical applications, was applied at $x = \ell$ with $\theta$ chosen to be the speed calculated for the slow traveling wave. With this boundary condition, the cable would be indistinguishable from an infinate length cable for a wave, steadily propagating to the right, with speed $\theta$. The computed wave train provided as data for this simulation has wavelength 1.91 cm, temporal frequency 124 Hz, and propagation speed 2.37 m/s for a temperature of 6.3°C. These parameters therefore lie on the slow branch of the dispersion relation with representation as in Figs. 1 and 3 but on the fast branch (near minimum wavelength) for Fig. 2. The results of this computation are summarized in Fig. 6. Fig. 6 *A* shows the trajectories of the pulses in the $x$–$t$ plane. Each point on this graph represents a crossing of a given voltage level (in this case 25 mV) at a distance $x$ cm from the left end of the fiber and a time $t$ ms following the beginning of the experiment; solid curves represent pulse upstrokes and dashed curves are for downstrokes. The slope of the curve containing a given point is therefore the reciprocal of the speed of the pulse at that point in

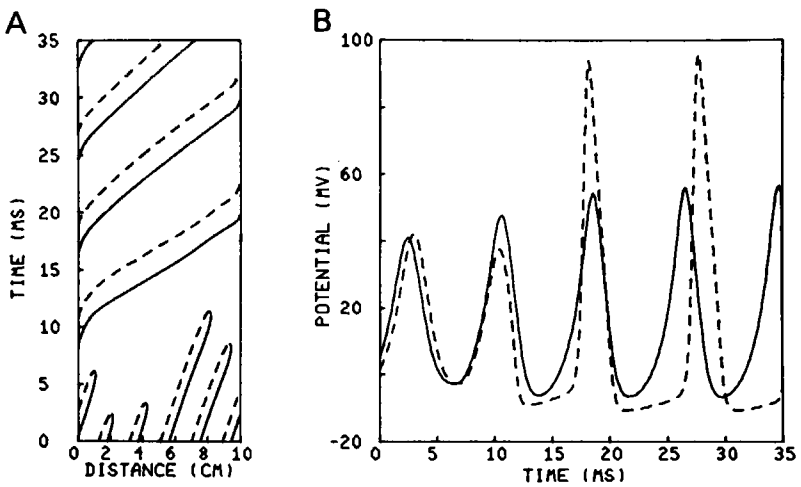


FIGURE 6 (*A*) Trajectories in the $x$-$t$ plane of upstrokes and downstrokes for successive pulses obtained from numerical solution of Hodgkin-Huxley cable equations. Each point on a solid curve represents an upcrossing of the 25-mV reference potential. The dashed curves are the downcrossing trajectories. A slow, presumably unstable, periodic wave train is given as the initial condition as well as the boundary condition at $x = 0$. Frequency, wavelength and speed for this input wave are 124 Hz, 1.91 cm, and 2.37 m/s, respectively; temperature 6.3°C. This wave persists only transiently and then appears to evolve into the faster, evidently stable, wave train of the same frequency. (*B*) Time profiles of the solution to the cable equation at $x = 0.25$ cm (solid) and $x = 8$ cm (dashed). Dashed and solid peaks that appear close to one another do not actually correspond. See text for details. MS, millisecond; MV, millivolt; CM, centimeter.

space and time. This representation is a common and useful one in the study of linear and nonlinear wave propagation. This figure shows the decay of the slow waves, followed by a regime in which the larger fast waves dominate. Those small amplitude pulses which started out on the fiber initially propagate from left to right with the slow speed 2.37 m/s predicted by the traveling wave calculation before the backs catch up with the fronts and the pulses collapse and disappear. The pulses which dominate the solution at later times begin slowly, speed up, and slow down again just as they approach the right end. This is due to the boundary conditions. Since the potential is constrained to follow the temporal pattern of the slow wave at the left end, it requires some finite interval in space and time to accelerate and to grow to full size. The behavior at the right end of the fiber can be interpreted in terms of the boundary condition, Eq. 6. Since $V_x/V_t$ is the slope of the contour in the $x$-$t$ plane on which $V$ is equal to a given constant, the boundary condition Eq. 6 may be viewed as the requirement that all constant voltage contours in the $x$-$t$ plane intersect the vertical line $x = \ell$ with slope $1/\theta$. Hence as a wave with speed $>\theta$ approaches the right end, it must slow down to meet this requirement.

At later times, the faster waves clearly predominate, but in this simulation, the stable periodic regime does not have time to evolve completely. Near $x = 2$, however, the third fast wave takes on a speed very close to that predicted for fast waves at this frequency, 124 Hz.

Fig. 6 *B*, which shows the time course of the potential at $x = 0.25$ cm (solid) and at $x = 8$ cm (dashed), must be examined with careful attention to Fig. 6 *A* for a correct interpretation, since the peaks in the dashed curve do not correspond to the nearest peaks in the solid curve. The first two smaller pulses on the dashed curve do not correspond to pulses that originated at the left end; rather they correspond to small amplitude pulses that were present in the initial conditions. These two small pulses persisted long enough to propagate past the sample point at $x = 8$ cm. This can be seen by noting that a vertical line drawn on Fig. 6 *A* at $x = 8$ cm intersects the leading and trailing edges of two waves which later decay. A further examination of Fig. 6 *A* reveals that the second small pulse in the solid curve grows into the first large pulse in the dashed curve.

## 3. STIMULUS-RESPONSE PROPERTIES OF THE MODEL FIBER

In this section we shall examine several computed solutions to the set of partial differential Eq. 1 in the light of our findings for the traveling wave Eq. 4. We have used the Crank-Nicolson finite difference method (see Appendix) to solve Eq. 1 with specified initial and boundary data. For each of the simulations of this section, the axonal segment spans $0 \leq x \leq \ell$ and the boundary conditions are

$$\partial V(0, t)/\partial x = -I_s(t) \cdot R/(\pi a^2)$$

and

$$\partial V(\ell, t)/\partial x = 0.$$

The condition at $x = 0$ corresponds to a time dependent stimulating current $I_s(t)$ ($\mu$A) while the condition at $x = \ell$ represents a sealed end. Initial conditions, for $t = 0$, were taken to be the uniform rest state.

As we pointed out earlier, the assumptions leading to Eq. 5 are rather specialized, and it

remains to be shown that these conditions are applicable to more realistic problems. Accordingly, we shall first present a sample calculation showing the relevance of the traveling wave hypothesis in one computational experiment. The traveling wave hypothesis, Eqs. 2 and 3, is exactly the assumption that the spatial and temporal profiles of the solution to the partial differential equation are identical in some space and time scales determined by $k$ and $\omega$ respectively. Fig. 7 shows spatial and temporal profiles, scaled appropriately, of a computed solution to Eq. 1 with temperature set at 18.5°C. The stimulus was periodic square current pulses injected at the left end of the fiber with high frequency of 358 Hz. The fiber was initially at rest. These profiles are compared with the corresponding periodic traveling waveform for their frequency (indicated by crosses). The three curves are barely distinguishable. We conclude that the traveling wave hypothesis is a good approximation for this frequency and over this time and distance range.

The following four figures are intended to illustrate the dispersive nature of impulse propagation for the Hodgkin-Huxley model and how asymptotic pulse speeds or changes in speed of individual pulses during propagation are predicted by the dispersion relation. Our first two experiments, for periodic stimulation, address the suggestion that maximum steady firing frequency has an upper bound $\omega_{max}$ as given by the dispersion relation.

At 6.3°C our findings presented in section 2 predict a maximum frequency of 147 Hz. Our simulations with stimulus frequencies just below the maximum show a 1:1 response of the fiber, i.e., a propagated pulse for each pulse of our square wave stimulus. For stimulus frequencies just above our predicted maximum frequency, we observe dropping of pulses and the failure of the model fiber to follow the stimulus faithfully. Calculations performed by

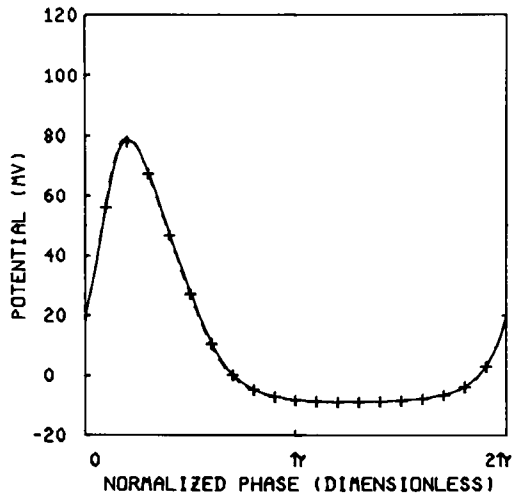


FIGURE 7 Superposition of temporal profile (dashed) of solution to the full cable equations, spatial profile (solid) of solution to the full cable equations, and a periodic traveling wave solution (crosses) which satisfies Eqs. 3 and 5. Stimulus for cable equations is periodic (358 Hz) square current pulses delivered at $x = 0$. Spatial profile is for $t = 19$ ms with $2.83 \leq x \leq 6.76$ (cm). Temporal profile is for $x = 5$ cm with $14.94 \leq t \leq 17.73$ (ms). Crosses represent traveling wave solution evaluated at every fifth point of a 100-point grid. This wave with temporal period 2.79 ms was calculated for given spatial period 3.93 cm ($k = 1.6$). Temperature, 18.5°C. MV, millivolt.

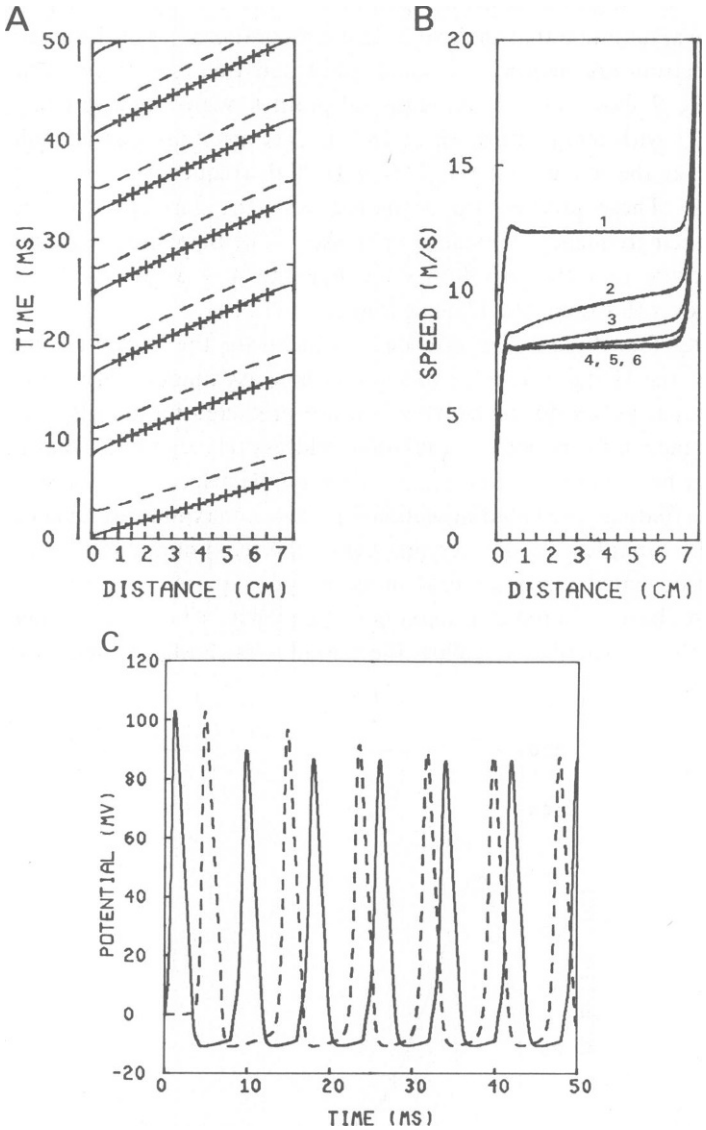


FIGURE 8 Response of model fiber, initially at rest, to 125 Hz periodic, square current pulse stimulus; temperature, 6.3°C. (*A*) Upstroke (solid) and downstroke (dashed) trajectories in $x$-$t$ plane of successive pulses. Vertical bars to the left of the vertical axis represent timing and duration of the stimulus. Crosses are for trajectories obtained by the approximation procedure of section 4. (*B*) Instantaneous speed of pulse upstroke vs. distance taken from trajectories in *A*. Speed of each succeeding pulse decreases from that of the solitary pulse to that of the steady wave train. Increase in speed near $x = 7.5$ cm results from sealed end boundary condition. (*C*) Temporal profiles of computed membrane potential at $x = 0.5$ cm (solid) and at $x = 5$ cm (dashed). MS, millisecond; CM, centimeter; M/S, meter/second.

Dodge and Cooley (personal communication) show similar behavior at 18.5°C for frequencies near 400 Hz, as did other calculations of ours which we do not present here. It should be noted that our predicted maximum frequencies are above those noted for the case of constant current stimulation (45) and would not be expected to be observed for the model or in the laboratory without time periodic stimulation. Figs. 8 and 9 represent results of simulations of a model axon 7.5 cm long, stimulated from the left with periodic square current pulses 10 $\mu$A in amplitude and duration indicated by vertical bars to left of ordinate axis in Figs. 8 *A* and 9

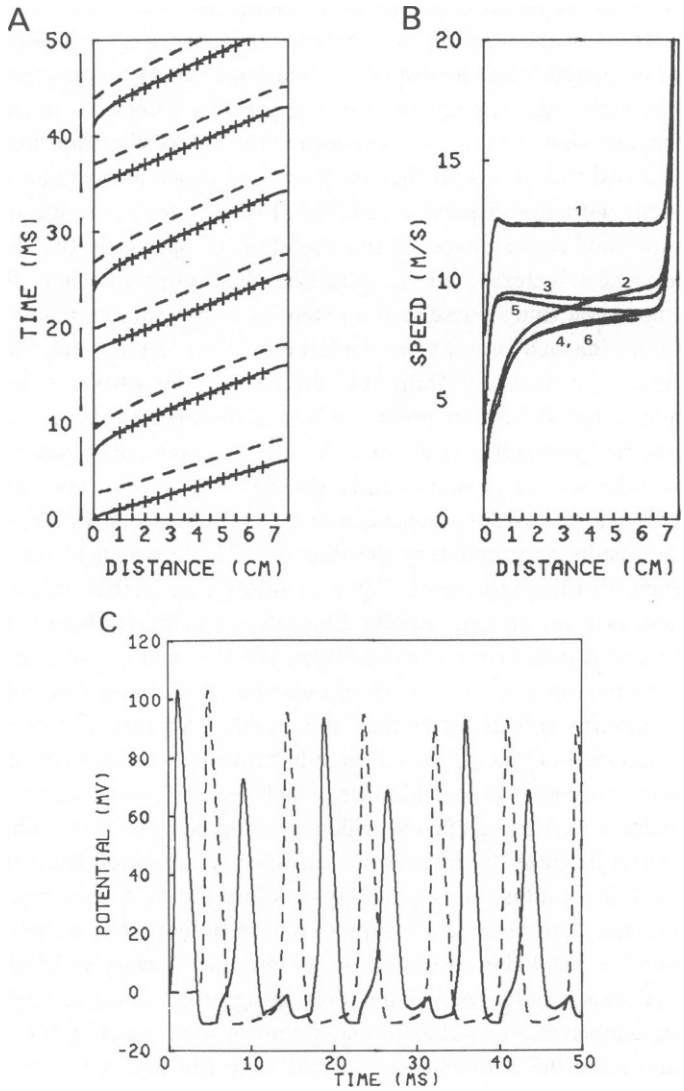


FIGURE 9 (*A-C*) Response of the model fiber to periodic square current pulses with frequency 175 Hz which exceeds $\omega_{max}$; temperature, 6.3°C. Graphic format same as Fig. 8. Every third stimulus fails to initiate a pulse. Even-numbered pulses accelerate while odd-numbered, nonleading pulses decelerate during propagation (*B*). Interspike intervals (*A*) and pulse amplitudes (*C*) tend to become uniform during propagation. MS, millisecond; MV, millivolt; CM, centimeter.

*A*. The sealed end condition at $x = \ell$ can be viewed as a special case of the boundary condition Eq. 6 in the preceding section, with the speed chosen to be infinite. Thus all of these impulses are observed to speed up as they approach the right end. Fig. 8 shows an example of stimulation at a frequency (125 Hz) near but below $\omega_{max}$. Fig. 8 *A* shows the trajectory of pulses in the *x-t* plane, the same representation as in Fig. 6 *A*. The first pulse, with an upstroke which arises from the rest state, travels at the speed of the solitary pulse. Succeeding pulses which propagate into regions of relative refractory left in the wake of their predecessors travel more slowly, as is evident from the increase with time of the slopes of the trajectories in Fig. 8 *A*. We plot the speeds of the pulses explicitly as a function of their progress along the fiber in Fig. 8 *B*. After <50 ms of model time, we observe convergence of the speeds of successive pulses to the value predicted from the dispersion relation (Fig. 1) for this frequency. During the transient phase, each pulse (except the first) accelerates somewhat during propagation. Because a pulse travels slower than its predecessor, the interspike time interval, since the preceding pulse, widens; this allows further recovery and hence an increase in speed. These effects are consistent with the dispersion relation (Fig. 1) for this range of instantaneous frequency. An important consequence of the evolution of speeds is the difference in the temporal pulse sequence at different points on the fiber. This phenomenon is illustrated in Fig. 8 *C*. This figure shows the time course of the potential at two sample points located 0.5 cm (solid curve) and 5 cm (dashed curve) from the left end. Near the left end, the spike intervals are very nearly uniform. At 5 cm from the left end of the fiber the beginning of the convergence of pulse intervals to that predicted by the dispersion relation can be seen. The interval between the first two spikes is the longest. The first spike propagates into a region of resting fiber, while the second is significantly slowed in its wake. The relative speeds of succeeding spikes change less as the pattern converges to the steady periodic wave profile.

Fig. 9 shows the results of stimulating the fiber at 175 Hz which is above the predicted maximum frequency. In this experiment, Fig. 9 *A* shows clearly that only two out of three current stimuli result in a transmitted impulse. Since the time interval between the second and third transmitted pulse is greater than that between the first and the second, the membrane has a greater time to recover and thus the third pulse initially travels faster than the second; similarly, the fifth initially travels faster than the fourth. This rather interesting pattern of speeds can also be observed in Fig. 9 *B*. The first pulse travels at the speed of the solitary pulse. As in the previous experiment, the second pulse, which starts slow speeds up as it propagates because the first pulse, which travels faster, widens the gap between them. The third stimulus fails to initiate a pulse because the fiber is not sufficiently recovered from the second. This effectively allows a full stimulus interval to elapse before the next pulse begins. The fourth stimulus gives rise to the third propagated impulse that initially travels faster than the second, but then slows down for awhile because it advances into the recovery wake of its predecessor faster than the predecessor pulls away. This alternating effect tends to make the temporal pulse spacing more uniform as the pulses propagate down the fiber. Fig. 9 *C* shows temporal profiles of the potential at 0.5 cm (solid curve) and 5 cm (dashed curve) to the right of the stimulus site. Here the different temporal sequences at different points on the fiber are clearly shown. The smoothing of the amplitude variation as the train of pulses propagates is also apparent here.

Fig. 10 shows the response to a slightly more complicated temporal stimulus pattern. The

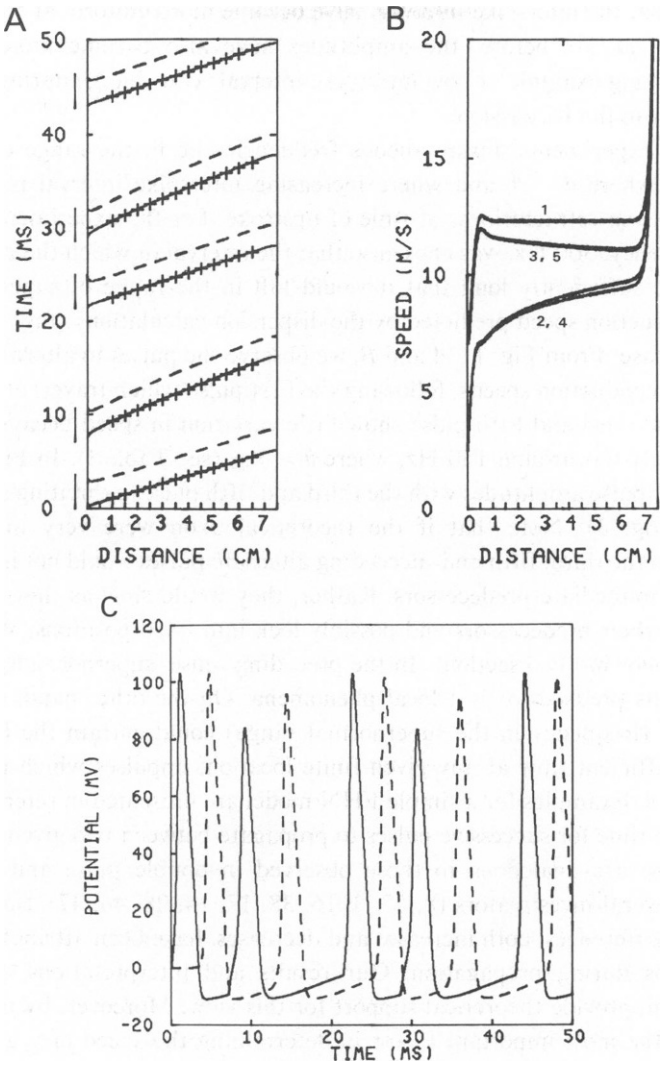


FIGURE 10 (*A-C*) Response of the model fiber to repetitive square current pulses with every third stimulating pulse omitted. The underlying stimulus frequency is 140 Hz; temperature, 6.3°C. The deliberate two-skip-one pattern at input is not well preserved during propagation (see also Fig. 12). MS, millisecond; M/S, meter/second; MV, millivolt.

basic stimulus frequency is 140 Hz (just slightly below the maximum frequency) but every third stimulating current pulse has been omitted. Again we notice that interspike intervals which follow the odd-numbered, and faster traveling, pulses are initially short and then tend to lengthen. Consequently, the even-numbered pulses encounter decreasing refractoriness and so accelerate during propagation. Conversely, the odd-numbered nonleading pulses, initially fast, decelerate as they come closer to their predecessors. The deliberate two-skip-one input pattern is not preserved during propagation. In a longer fiber, and perhaps after a longer time, we would expect to see the pulses approach uniform temporal spacing. The profiles of Fig.

10 *C* also show that the interspike intervals have become more uniform at 5 cm from the left end than at 0.5 cm. As before, the amplitudes have also become more uniform. This experiment, a striking example of how interspike intervals can change during propagation, is considered further in the Discussion.

For the above experiments, instantaneous frequencies lie in the range of the dispersion relation (Fig. 1) where $\theta < \theta_f$ and where increasing interspike interval implies increasing speed, and decreasing refractoriness at time of upstroke. For the experiment of Fig. 11, the stimulating frequency, 300 Hz, was chosen so that the interval in which the current pulse was skipped would be sufficiently long that it would fall in the range of superexcitability and supernormal conduction speed predicted by the dispersion calculations (Fig. 1). Temperature is 18.5°C in this case. From Fig. 11 *A* and *B*, we observe the pulses to alternate between sub- and supernormal conduction speeds, following the first pulse which travels at the speed of the solitary pulse. The third and fifth pulse show little variation in speed because the dispersion relation is relatively flat around 150 Hz, where $\theta \approx \theta_{max}$ (see Table I). In Fig. 11 *C* one also sees alternation of pulse amplitudes with the third and fifth pulses exhibiting supernormal size (compare with Fig. 3). Note that if the theoretical axon were very much longer, say semi-infinite, then the third, fifth and succeeding alternate pulses would not indefinitely travel faster than their immediate predecessors. Rather, they would slow as they encountered the recovery wake of their predecessors and possibly lock into fixed positions. We return to this question in the following two sections. In the preceding sense, supernormal propagation of a pulse relative to its predecessor is a local phenomena. On the other hand, uniformly timed repetitive stimuli (frequency in the supernormal range) could entrain the fiber so that one observes, after sufficient time at any given finite location, impulses which propagate at the supernormal speed. Examples for a simple FHN model are presented in reference 43.

The changes in time for successive pulses to propagate between two given locations, in the above simulations, are analogous to those observed in double pulse and repetitive pulse experiments of several investigators (8, 37, 3, 16, 38, 17, 14, 28, 46, 47). Such experimental conduction time differences, both increases and decreases, have been attributed to changes in conduction speeds during propagation. Our results and interpretations, in terms of the dispersion relation, provide theoretical support for this view. Moreover, by making the naive supposition that the most important factor in determining the speed of a given pulse is the time that has elapsed since the preceding pulse, one might use our calculated dispersion relation to predict the instantaneous speed of a given pulse. The most obvious consistency check on this assumption is trivially fulfilled: if the time elapsed since the most recent pulse is infinite, i.e., the fiber is at rest, then a pulse will travel at the speed of the solitary pulse. In the next section we shall construct a mathematical formulation of this simple hypothesis and offer empirical evidence to support its quantitative validity.

## 4. AN APPROXIMATION TO DESCRIBE CHANGING INTERSPIKE INTERVALS DURING PROPAGATION

In section 2 we computed a family of periodic wave trains of uniformly spaced pulses whose speed is specified by a single parameter, e.g., frequency or wavelength. Furthermore, for the lower to intermediate frequency trains, the ($V$, $m$, $h$, $n$) trajectories may be approximately described by this single parameter as well; it roughly indicates the duration of the phase spent

on the common recovery pathway between pulses. Here we will apply these observations to individual pulses of a train in which their spacing is not necessarily uniform. We will provide approximate $x$-$t$ trajectories of the pulse upstroke positions for the stimulus-response simulations of the preceding section.

Our approximation procedure rests on the following assumptions: (*a*) Successive pulses

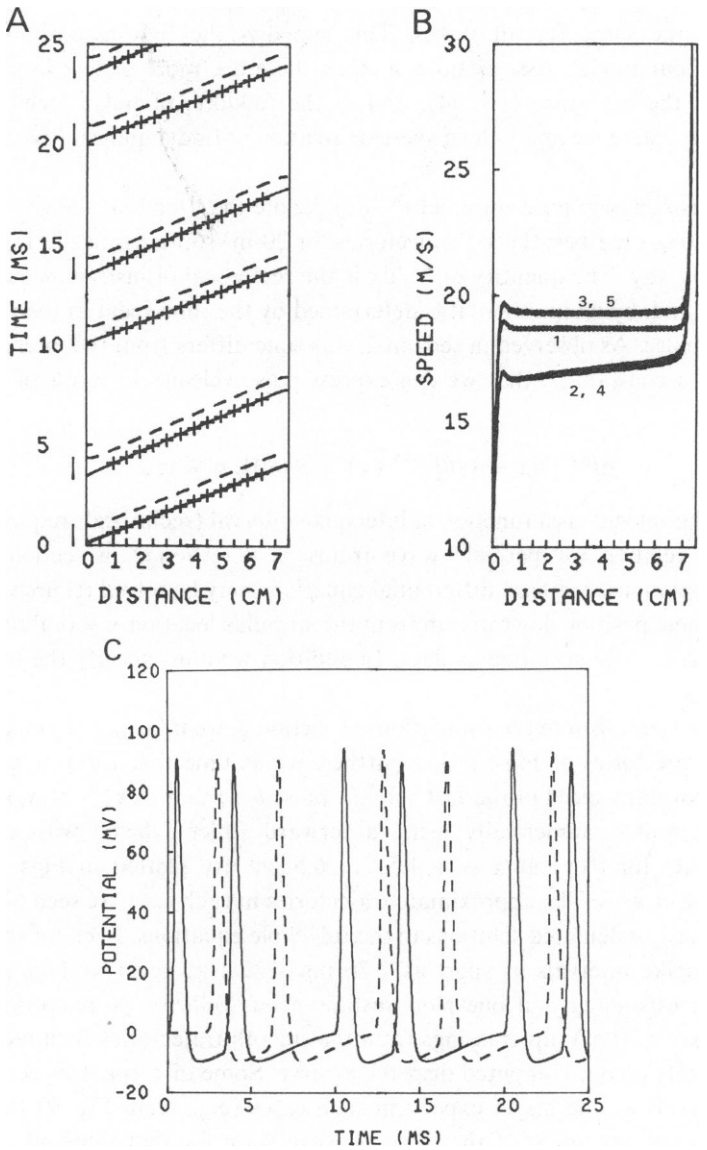


FIGURE 11 (*A-C*) As in Fig. 10 but with timing of pulses chosen so that the time interval in which stimulating pulse is omitted corresponds to a frequency for which the dispersion relation (Fig. 1) predicts supernormal conduction speed. The underlying stimulus frequency is 300 Hz; temperature, 18.5°C. Transmitted pulses alternate between sub- and supernormal speeds. MS, millisecond; M/S, meters/second; CM, centimeter; MV, millivolt.

follow a common recovery path after the spike downstroke; only duration along this path varies between pulses. (*b*) The speed of an individual pulse is determined primarily by the recovery wake of the immediately preceding pulse and this speed is given approximately by the dispersion relation. (*c*) Pulse arrival times at a location just downstream from the stimulus are provided as data. Explicit effects of stimulus and boundary conditions are not taken into account.

We observe in Fig. 4 that the total duration of spike upstroke, downstroke, and shoulder is approximately the same for all spikes. This supports the first assumption above in the formulation of our model. Assumptions such as these are more or less implicit in heuristic descriptions in the literature (16, 44), and in the folklore, of pulse speed dependence on previous activity. Here we apply the dispersion relation to find a quantitative estimate of local pulse speed.

For our approximation procedure, let $t^{n+1}(x)$ denote the time that the $(n+1)-st$ pulse is at position $x$ along the fiber; the $x$-$t$ trajectories for 20-mV up-crossings in Figs. 8–11 may be represented this way. The quantity $dt^{n+1}/dx$ is the reciprocal of instantaneous velocity of the pulse upstroke and, by assumption, it is determined by the time spent in the recovery wake of the preceding pulse. As observed in section 2, this time differs from the interspike interval by approximately a constant so that we can express pulse velocity in terms of interspike time. Thus we have

$$dt^{n+1}/dx = 1/\theta[t^{n+1}(x) - t^{n}(x)], \quad n = 1, 2, \ldots, \tag{7}$$

where $\theta[\cdot]$ is the velocity as a function of interspike interval (reciprocal frequency) as given by the dispersion relation for periodic wave trains as determined in section 2. This set of nonlinear, autonomous, ordinary differential equations may be solved recursively for $x \geq x_0 > 0$ where $x_0$ is some position downstream from the stimulus location $x = 0$. Pulse passage times $t^{n}(x_0)$, $n = 1, 2, \ldots$, are specified as data. In addition we must specify the trajectory for the first pulse $t^{1}(x)$.

To apply this formalism to the simulations of section 3, we take $x_0 = 1$ cm and obtain $t^{n}(x_0)$ from the $x$-$t$ trajectories of Figs. 8–11. Further, we assume that for $x \geq x_0$ the first pulse travels at the constant speed of the fast solitary pulse $\theta_f$ so that $t^{1}(x) = t^{1}(x_0) + (x - x_0)/\theta_f$. Eq. 7 was integrated numerically using a forward Euler scheme with $\Delta x = 0.05$ cm. Computed values for $t^{n}(x)$ at $x = 1, 1.5, \ldots, 6.5$ cm are plotted in Figs. 8 *A*–11 *A* and indicated by the crosses. The approximate trajectories in each case are seen to agree very well with our previously calculated solutions to the full cable equations. Even for the case of Fig. 9, in which interspike intervals as short as 7.76 ms (129 Hz) occur at 1 cm, the results are consistent. Correspondingly, if one plots instantaneous velocity vs. reciprocal time interval between successive 20-mV up-crossings from the smooth trajectories then most of these data fall approximately on our computed dispersion curve. Some discrepancies occur for the lower interspike intervals as one might expect; in such cases (e.g., from Fig. 9) the instantaneous velocity falls below the speed of the periodic wave train for that interspike interval. These explicit comparisons illustrate that the approximation procedure provides a reasonable estimate for the variation in interspike interval and the influence of dispersion during propagation. Moreover, it requires observations at only a single location provided, of course, that the dispersion relation is known.

This formal procedure we feel is successful primarily because pulse recoveries over a large frequency range follow a common pathway as pointed out in section 2. If, instead, pulses with different speeds had different wakes, then one would require a more general expression for the right hand side of Eq. 7. It would have at least two arguments. For example, the first might indicate that the nth pulse with speed $(dt^n/dx)^{-1}$ produces its individual recovery wake while the second argument might specify time spent along that path; thus $\theta = \theta(dt^n/dx, t^{n+1} - t^n)$. Approximation recipes for constructing upstroke trajectories in terms of a single parameter description of pulse speed as a function of previous recovery state have also been given by Keener (26) and Peskin (36). By singular perturbation methods for simplified, two-variable nerve models, these investigators exploited the assumption of an extremely slow time scale for the recovery variable to indicate how upstroke speed is determined. This also enabled them to describe the upstroke, downstroke, and shoulder or plateau of the pulse. Here, without explicit time scale assumptions, we utilize the numerically computed dispersion relation for the full HH model and the fact that pulses with long interspike intervals follow the trajectory of the solitary pulse. Explicit comparison of our results with those for approximate HH models, which are based on exaggerated time scale differences (e.g., $h$ and $n$ very slow relative to $V$ and $m$), would be informative. Such time scale assumptions for the HH model have been employed in various theoretical studies (11, 4, 5, 19, footnote 1) but not yet to calculate approximate dispersion relations or $x$-$t$ trajectories.

As mentioned above, our procedure is inaccurate at higher frequencies. Also, it is not appropriate to describe boundary and stimulus effects. These may lead to propagation failure (e.g., dropped pulses) and pulse collisions (e.g., sealed end boundary condition). To treat such phenomena one would need a more microscopic approximate description for pulse upstroke, shoulder, and downstroke. We have also neglected effects of succeeding pulses. This is reasonable for the lengths of model axons considered here, but for very long axons along which several pulses may propagate simultaneously, the possibility that a pulse may affect its predecessor(s) cannot be ruled out. Indeed, Evans et al. (private communication),[3] Feroe (10) and Carpenter (5) find theoretically, although by different arguments and mechanisms, that some finite trains of pulses, locked together with fixed speed, should travel faster than a solitary pulse.

While aware of the aforementioned restrictions, one might push the approximate recipe and ask about ultimate ($x \to \infty$, $t \to \infty$) steadily propagating interspike intervals consistent with Eq. 7 for a model axon of semi-infinite length. As idealizations one might seek these as equilibrium solutions of Eq. 7 with $dt^{n+1}/dx$ equal to a constant. For example, an ultimate state which is periodic with uniformly spaced pulses traveling at the same constant speed would have, according to Eq. 7, this speed and interspike or frequency related through the dispersion relation. For our computed examples this frequency for an equilibrium candidate would be the mean frequency of pulses initiated at $x = 1$ cm:125, 350/3, 280/3, 200; the last three figures being two-thirds of the input frequency.

While the $x$-$t$ and $\theta$-$x$ trajectories of our first two examples are reasonably consistent with

[3]Their work, not in manuscript form when this paper was submitted, is described in Evans, J. W., N. Fenichel, and J. A. Feroe. 1980. Double impulse solutions in nerve axon equations. *SIAM J. Appl. Math.* In press.

such a prediction, it is not obvious that the last two cases lead to uniform spacing. The ultimate state may be pulses locked in pairs. It is possible to formally construct periodic locked patterns for a model whose speed vs. frequency dispersion relation (fast branch) is not monotone. For example, in Fig. 1, for each speed in a supernormal range there are at least two different interspike intervals. Each such pair of intervals yield a mean frequency if one interval is considered the interburst interval and the other an intraburst interval. If the range of such mean frequencies includes the mean input frequency then this formally constructed periodic pattern is a candidate for an equilibrium solution to Eq. 7. A suitable candidate should also be a stable periodic pattern but this issue, a subtle one for the periodic case, will not be pursued here.

Rather, we consider the possibility of locking for a finite pulse train, say two pulses. Suppose the first pulse has speed $\theta_f$. Then, it follows from Eq. 7, that the interval $T(x) = t^2(x) - t^1(x)$ satisfies

$$dT/dx = 1/\theta(T) - 1/\theta_f. \tag{8}$$

Any interspike interval, call it $T_f$, for which the dispersion relation has $\theta = \theta_f$ is a possible equilibrium solution to Eq. 8; e.g., from the values of $\omega(\theta_f)$ in Table I: 16.0 ms for 6.3°C, 4.81 ms for 18.5°C, and 2.58 ms for 26°C. Note that such a possibility exists only if there is some range of supernormal speeds. Moreover, there may be several candidates if $\theta$ exhibits damped oscillatory behavior as $\theta \to \theta_f$ for $\omega \to 0$. Stability of any such equilibrium locking interval might be considered by perturbing $T_f$, $T(x) = T_f + \delta(x)$, and linearizing Eq. 8 to get

$$d\delta/dx = -[\theta^{-2}d\theta/dT]\delta, \tag{9}$$

where the term in brackets is evaluated for $T = T_f$. If $d\theta/dT < 0$, the pattern is unstable but presumably stable if $d\theta/dT > 0$ as in the above numerical examples from Table I. Similar qualitative observations have been made, but without explicit demonstration, by Karfunkel and Kahlert (25) for locked patterns in a system with a nonmonotone dispersion relation. The results are also consistent with Feroe's (10) analysis of stability for finite pulse train solutions to a simple FHN type equation. See Rinzel (43) for further discussion, applications, and extensions of the approximate pulse kinematics, which we introduced in this section.

## 5. DISCUSSION

In the previous four sections, we have described the results of a series of numerical experiments in which we first computed periodic traveling wave solutions to the HH equations, investigated the detailed features of these solutions and then explored their application to the solution of more general signaling problems. For the periodic wave trains, we found a dispersion relation with two branches, one fast and one slow, with predicted speeds of the pulse trains approaching the known speeds of the fast and slow solitary pulses as the frequency decreased to zero. On the fast branch, we saw speed and amplitude decrease with increasing frequencies in the higher frequency ranges, with a range of intermediate frequency wave trains with supernormal conduction speeds. Our findings also confirmed the widely held intuition that the duration of the recovery phase essentially determines the period of the wavetrain. The underlying recovery time course was found to vary little with frequency over a

broad range of low to intermediate frequencies. The primary distinguishing feature of these wave trains is time duration along the approximately common recovery pathway. This in turn determines the degree of recovery at pulse upstroke and, hence, speed and amplitude of the periodic pulse train. Moreover, we observed that, while the periodic traveling wave solutions do not resemble in detail periodic solutions to the space clamped HH equations with constant current stimulation (see reference 42 for these solutions), the recovery trajectory does resemble that of a space clamped action potential that is initiated by an instantaneous depolarization. This fits our intuition that the common recovery path is determined by membrane characteristics rather than effects of spatial dependence, since the space derivatives of the potential are small during the recovery phase.

We remark that certain of these features of the traveling wave solutions may be exposed analytically by the method of singular perturbations but at the expense of assuming that $h$ and $n$ are relatively very slow processes. In the lowest order approximation, one studies reduced systems to construct a solution in four pieces: a rapid upstroke during which $h$ and $n$ are constant, a slow (but short for the HH case) plateau, a rapid downstroke with $h$ and $n$ constant, and a slow recovery phase. The recovery state, i.e., the values of $h$ and $n$, at the upstroke determine the propagation speed. During the slow plateau and recovery, cable properties are neglected and space-clamped dynamics, with $V$ and $m$ at equilibrium, determine the trajectory. Carpenter (4, 5) has exploited these methods for qualitative studies while Hassard[1] calculated the lowest order HH solitary pulse solution in this approximation. Casten et al. (6), had earlier carried out the procedure for the FHN model. In our numerical method, the upstroke, plateau, and downstroke are fit implicitly rather than explicitly; we solve the full equation without assumptions of exaggerated time scales. We expect the characteristics described in the preceding paragraph to be generally applicable to low frequency wave train solutions of nerve conduction equations. They depend not necessarily upon widely differing time scales for the membrance dynamics but rather upon the approach of the recovery trajectory in its late phase to the vicinity of the rest state (see reference 43 for further discussion).

As we have observed, periodicity per se of the low to intermediate frequency wave train solutions does not significantly alter the recovery time course. Therefore one might expect to view a transient, not necessarily periodic or steadily propagating, wave train as a sequence of similar recoveries interrupted at varying points by upstroke-downstroke pulses. Each pulse, along with the recovery path since its predecessor, would be interpreted as a single cycle of the periodic wave train with the corresponding period or duration. Instantaneous speed of a pulse is obtained from the dispersion relation by interpreting time since the preceding pulse as the reciprocal of instantaneous frequency. In section 4 we incorporated this observation into a simple kinematic model of the propagation of an individual nerve impulse in a train. The dispersion relation is the only physiological information contained in this simple model. The success of this model in predicting the time course of pulse propagation in several signaling problems (cf. Figs. 8–11) where the periodic traveling wave hypothesis is not rigorously valid is evidence that the dispersion relation contains a great deal of information about the propagation characteristics of the nerve.

We would like to consider our results as quantitative predictions of pulse dispersion in the squid giant axon viewed as an experimental model. The most direct application is to the

relation of speed to frequency during repetitive firing, the temperature dependence of this relation, and the maximum frequency for sustained propagation. We are reminded (J. W. Moore, private communication; see also reference 1) that the repetitive state may be an idealization not easily realized in squid, for example, because of potassium accumulation. Nevertheless, our results show that the dispersion relation should further apply to predict, approximately, the changes in conduction speed and interspike interval during propagation of individual pulses of a train, for example, even for a two-pulse train.

More generally, beyond the case of squid, dispersion is a qualitative feature of nerve models, which arises from the nature of the recovery time-course. Only the degree of dispersion varies from model to model. The fact that a dispersion relation had been found for simplified models (41, 6) was part of the motivation for this study.

Because dispersion is a general phenomenon, one is motivated to ask about its effects upon temporal coding. In a fiber which transmits temporally coded information, a change in interspike intervals represents a change in information. (This observation has also been noted by George [16] and Swadlow and Waxman [46].) George (16) also studied the effects of dispersion on statistical properties of spike trains. Such changes in temporal sequences have been observed in preparations in which temporal coding was claimed (17). Our numerical simulations show quantitative examples of this phenomenon for the HH model. Fig. 12 is derived from the same calculations from which Fig. 10 was produced. This figure shows directly the changes in interspike interval as the pulses progress down the fiber. In a fiber that carries purely temporally coded information, one would expect the ratios of interspike intervals to be preserved. In this example we see a ratio of 2:1 at input become the altered ratio of $\approx$6:5 near the far end, i.e., for the last two intervals measured at 6.5 cm. It is then reasonable to ask how encoding/decoding might be accomplished in this environment. In this regard we note that, if one knows the dispersion relation, the kinematic approximation presented in section 4 could in principle be used to reconstruct the pattern at $x = x_0$, from the pattern at $x = \ell$, by integrating Eq. 7 backwards.

Several investigators (8, 38, 37) have reported on two-pulse experiments, in which the speed of the second pulse is measured and recorded as a function of interspike interval. In these experiments the propagation speed $\theta$ is inferred from the conduction time over a known distance, typically between two separated locations; thus an average speed is measured. Therefore, in principle, close agreement with our dispersion calculations cannot be expected, especially for firing frequencies in ranges of the dispersion curve where $\theta$ changes rapidly with $\omega$.

Methods such as the one we outlined in section 4 can be used to predict the conduction time differences for two-pulse experiments from the dispersion curve. However, in general, it is not clear how to solve the converse problem of calculating the dispersion relation from the results of two-pulse experiments with measurements at only two separated locations. If, on the other hand, observations are available at several closely spaced locations, then better estimates of instantaneous speed and interspike interval would be obtained. Since these instantaneous values approximately satisfy the dispersion relation, for the low to mid-frequency range, one would have an estimate for that relation.

Finally, we would like to examine briefly the subject of pulse locking for a wave train, i.e., the stabilization of pulse speed to a fixed value and interspike intervals to fixed, but not

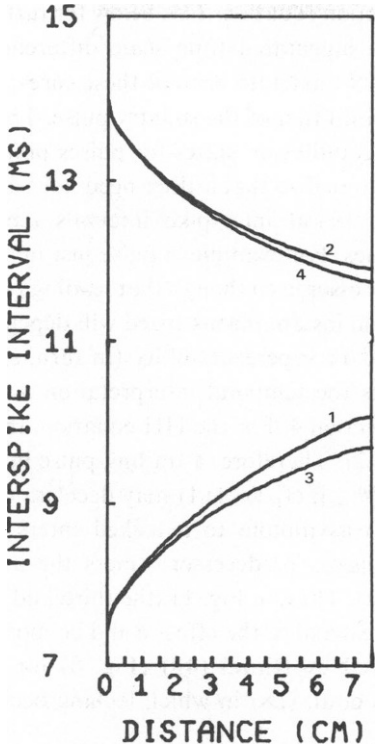


FIGURE 12 Changes in temporal interspike interval as the pulses propagate along the model fiber, in the calculation for Fig. 10. Numbers denote the sequence of interspike intervals. Intervals alternate between smaller and larger, due to the dropped pulses. Ratio (2/1) of interstimulus intervals is not transmitted by pulses but rather leads to greatly reduced ratio (6/5) of interspike intervals after propagation. MS, millisecond; CM, centimeter.

necessarily equal, values. Karfunkel and Kahlert (25), Donati and Kunov (8), and Scott and Luzader (44) have presented heuristic arguments for a pulse locking mechanism based on a nonmonotone dispersion relation. They argue, for the two-pulse case, that pulse spacing (or, alternatively, interspike time interval) will stabilize at a value for which speed on the $\theta$ vs. $P$ (equivalently, $\theta$ vs. $1/\omega$) curve equals that of the solitary pulse, provided that $\theta$ increases with $P$ (equivalently, $1/\omega$) at that point. (We have tabulated these frequencies for our calculated dispersion relations in Table I.) The reason is that for such a point on the dispersion curve, pulses with slightly longer spacing will go faster than $\theta_f$ and pulses with slightly shorter spacing will go slower than $\theta_f$. Thus if one pulse in a train moves slightly closer to the pulse ahead of it, and thus slightly further from the one behind it, two things will happen: the pulse in question will slow down, and the one immediately behind it will speed up, thus tending to restore the original situation. Our kinematic approximation presented in section 4 contains a mathematical formalization of the above intuition in Eqs. 8 and 9. In the case of a two-pulse experiment on a long fiber, this approximation suggests that the first pulse would travel at the speed of the solitary pulse and the second pulse would, asymptotically, travel at the same speed and fixed distance behind the first one. The existence of such finite pulse train traveling wave solutions has been demonstrated by Evans, Fenichel, and Feroe (private communica-

tion) for a class of nerve conduction equations (see below for further details), by Carpenter (5) for HH type equations with exaggerated time scale differences, and by Feroe (10) with explicit calculations for an FHN model. In each of these cases, a stable finite pulse train has speed close to (actually exceeding) that of the solitary pulse. These solutions are idealizations of asymptotically approached equilibrium states for pulses propagating on an infinitely long fiber. It is important however to realize that a fiber need not be long relative to pulse spacing (in $x$) for one to observe temporal interspike intervals tending transiently toward the corresponding equilibrium values. For example, a pulse just initiated is still influenced by the long recovery wake of its predecessor even though that leading pulse might have propagated to the axon's far end. The effect on instantaneous speed will depend on conduction time and the degree of variation of sub- and/or superexcitability (in turn, speed) with duration into that wake. This remark emphasizes the temporal interpretation of the dispersion relation ($\theta$ vs. $1/\omega$) as do the kinematics of section 4. For the HH equation, the supernormal speed hump is shallow and wide (Figs. 1 and 2). Therefore, a trailing pulse initially timed to have maximal supernormal speed ($\Delta t = 1/\omega[\theta_{max}]$; cf. Table I) may decelerate only slightly toward speed $\theta_f$ and exhibit little tendency to asymptote to a locked interspike interval (e.g., kinematic prediction of $1/\omega[\theta_f]$) following its predecessor, unless the axon were quite long (tens of centimeters for the 18.5°C case). Thus, in Fig. 11, the third and fifth pulses show little change in speed. For other models or real axons, the effect could be more or less significant; a striking theoretical example is described by Rinzel (43) (Fig. 8) for a FHN model; also, see the experimental results of Kocsis et al. (28) in which locking occurs over physiological lengths (<1.5 cm.).

The above kinematic mechanism for pulse locking, the supernormal speed hump, follows from the overshoot or oscillation between sub- and superexcitability as the recovery trajectory of the solitary pulse approaches the rest state (see section 2, also reference 28). The ultimate approach is described from the linearization about rest of the traveling wave equations with speed $\theta_f$. Evans et al.[3] have rigorously proven, under the assumption that the slowest decaying mode of this linearization is a damped oscillation, that finite pulse train solutions (locked patterns) exist. A locking position corresponds to a pulse upstroke which occurs during a phase of its predecessor at which the damped oscillation swings through either super- or subexcitability and which thereby gives rise to locking positions that are either stable or unstable (similar suggestions are made based on experimental observations[4] in reference 48). Hence locking occurs at multiples of the half-period of the damped oscillation. Moreover, there are an infinite number of different finite pulse train solutions; for example, the different two pulse solutions have spacings which correspond to different multiples of the half-period. These rigorous results are asymptotic, for large interspike intervals. Nevertheless, Feroe (10) finds, for his computed two-pulse FHN solutions, that the difference between the separation from the first to the second pulse in the two patterns of closest spacing agrees approximately with the linearization half-period. For the HH solitary pulse, the return to rest is a damped oscillation but only at higher temperatures; at 6.3°C, there is, however, a detectable overshoot in excitability with the return to rest. It is worthwhile to relate our numerical results to the

[4]Waxman et al. (48), however, did not detect supernormal speeds or excitability in their computer simulations of a noded axon using a modified HH membrane model.

Evans et al.[3] description and, in doing so, we offer an interpretation based on the dispersion relation (see also references 43, 25).[5] Intuitively, one might expect of the dispersion relation as $\omega$ tends to zero, that $\theta$ approaches $\theta_f$ through a sequence of damped supernormal-subnormal swings with period equal to that of the solitary pulse oscillatory return to rest (this remains to be rigorously demonstrated). The supernormal hump we have calculated would then represent a single local speed maximum. Given this, the kinematic approximation would then predict many different finite pulse train solutions with interspike intervals corresponding to the various values of $\omega$ for which $\theta(\omega) = \theta_f$; some intervals would be stable and some unstable depending on whether $d\theta/d\omega < 0$ or $>0$, respectively. The computations presented in section 2 do not extend with sufficient refinement for adequately low frequencies to evaluate these intervals precisely and to verify this hypothesis in quantitative detail for the HH equations. Our dispersion curves (Figs. 1 and 2) for 18.5° along with more recent calculations exhibit small subnormal swings and allow for an approximate comparison (analogous to Feroe's) with reasonable agreement between the linearization period and the spacing interval for two-pulse solutions (here, predicted by kinematics).

## APPENDIX

### *Numerical Methods*

FOR PERIODIC TRAVELING WAVE SOLUTIONS One procedure for solving Eq. 5 with boundary conditions Eq. 3 would be: after fixing values of $k$ and $u$ at $z = 0$, guess $\omega$, along with the values of $u'$, $p_1$, $p_2$, and $p_3$ at $z = 0$. These guesses define an initial value problem for the system Eq. 5 which may be solved by some standard method, e.g., Runge-Kutta or Cauchy-Euler for the interval $[0, 2\pi]$. The resulting values of $p_1(2\pi)$, $p_2(2\pi)$, $p_3(2\pi)$, and $u'(2\pi)$ could then be used to refine the estimates of $\omega$, $p_1(0)$, $p_2(0)$, $p_3(0)$, and $u'(0)$. This process could, in theory, be repeated until a periodic solution is obtained to the desired degree of accuracy. In the numerical analysis literature, this method is known as a shooting method (see for example reference 24). Such a method was used by Hodgkin and Huxley (20) in their original calculation of the solitary pulse. Evans and Feroe (9) and FitzHugh and Antosiewicz (3) also used shooting methods in their calculations, as did Huxley (22). In these, and other similar problems,[6] although shooting may be satisfactory for determining the speed of the solitary pulse, it is probably impractical for computing the solution profile. This is because the solution at the right hand end point is extremely sensitive to the estimate of speed (equivalently, $\omega$). FitzHugh and Antosiewicz (13) exhibit a case in the computation of the solitary pulse in which two estimates of the speed which agree to eight decimal places lead to two solutions to the initial value problem which diverge, one strongly positive, the other strongly negative, before the completion of the downstroke. Similarly, shooting is not practical for finding periodic solutions since reasonable values are required at the end of the interval in question and a reasonable solution to the initial value problem cannot be obtained without

[5]To characterize locking in terms of the dispersion relation or finite pulse train traveling waves may have some advantage in precision over the conceptual characterization in terms of excitability during recovery. The former is a stimulus-independent description for well-defined, particular solutions while the latter is not.

[6]Miura, R. 1979. Accurate computation of traveling wave solutions. I. The FitzHugh-Nagamo equation: stable solitary wave. Preprint.

unreasonably accurate estimates for the frequency $\omega$ of the pulse train, and for the initial conditions $p_1$, $p_2$, $p_3$ and $u'$ at $z = 0$, along with an also unreasonably accurate solution to the system of ordinary differential Eq. 5. The root of the problem is that there is no guarantee that the desired periodic solution is stable as a solution to Eq. 5, regardless of its stability as a solution to the cable Eq. 1. If it is not stable, some small error in the initial condition or in shooting may displace the approximate solution trajectory away from the periodic solution and on to a divergent one. These difficulties are described in detail by Rinzel and Miller (42).

To avoid this difficulty we do not transform Eqs. 3 and 5 to an equivalent initial value problem; rather, we deal with it directly as a two point boundary value problem (see reference 40 for a preliminary report). Miura[6] has also posed the calculation of the solitary pulse as a boundary value problem. To calculate an approximate periodic solution, we use a finite difference method, which is presumably insensitive to the stability of the desired orbit. In our computations, we impose a grid on the interval $[0, 2\pi]$ with uniformly spaced grid points: $z_j = j\ 2\pi/N$, $j = 0, 1, \ldots, N$. We replace the derivatives in Eq. 5 by any one of several finite difference approximations. The finite difference formula couples the values of the solution at nearby points, and the periodicity condition is used to evaluate the difference formula at those points which are coupled to points outside the interval $[0, 2\pi]$. This finite difference formulation thus leads to a large system of coupled nonlinear equations for the discrete solution. There are $4N$ equations: four equations at each of the $N$ points (recall that there is only one endpoint, since 0 and $2\pi$ are regarded as identical). However, this system of nonlinear equations does not have a unique solution. Given any solution, we may derive a distinct solution by simply translating the entire interval and its corresponding solution values one grid interval to the left, and then taking that grid interval that fell to the left of zero and placing it at the far right. We avoid this translation difficulty by arbitrarily fixing $u(0)$ to some value the membrane potential will assume during a cycle. Thus for the $4N$ equations we have $4N$ unknowns: the values of $u$, $p_1$, $p_2$, and $p_3$ in the interior, the values of $p_1$, $p_2$, and $p_3$ at $z = 0$, and $\omega$. This system can be solved by Newton's method or by a secant method. In some cases we found it convenient to define a new variable:

$$w = u',$$

and replace the first part of Eq. 5 with

$$\begin{aligned} u' &= w \\ k^2 w' &= w + I_i(u, p_1, p_2, p_3). \end{aligned}$$

In this case we have $5N$ equations in $5N$ unknowns. The grids used in these calculations contained 100 to 500 grid points. For computational efficiency special techniques were usually employed to solve the large linear systems that occur at each step of Newton's method for these problems. We have checked this method by using it to reproduce the dispersion relation for a simplified and analytically solvable FHN type nerve model (41). We have also observed good agreement between the results of this method and the computed solutions to the partial differential equations with appropriate boundary conditions; an example appears in Fig. 8.

For most of the results described here, we used backward difference formulas (either third or fifth order) chosen from those implemented in Gear's (15) package for stiff ordinary differential equations. Originally we had used a centered difference scheme and experimented

with nonuniform grids, but we encountered stiffness instabilities in the computation of traveling wave solutions to the cubic FHN equations. These problems disappeared when the centered scheme was replaced with one of the backward difference schemes.

Typically, in our computations we replaced the first entry in the solution vector, i.e., the place that $u(0)$ would have occupied had we not arbitrarily fixed it, with the unknown parameter $\omega$ or $k$. Solution of this problem (in the form Eq. 11 with Eq. 5) by Newton's method requires solving a set of linear equations, at each step, whose coefficient matrix (the Jacobian matrix) J has the block form:

where each asterisk represents a $5 \times 5$ matrix and all other elements are zero. The diagonal and subdiagonal blocks arise directly from the difference equations. The block in the upper right hand corner arises from the application of the periodic boundary condition to the difference equations. The left border represents the unknown parameter either $\omega$ or $k$. This example is for a first-order (Euler) backward difference formula; for a higher order formula there would be more subdiagonal blocks in each row and more blocks in the upper right hand corner.

To solve the linear equations for the Newton update one might consider Gaussian elimination (24). This algorithm with partial pivoting, a technique of matrix row interchanges to enhance numerical stability, would not in general preserve the sparse structure of this matrix but could require considerable storage and computing time. Instead, the Sherman-Morrison-Woodbury (SMW) procedure (21) can be used to advantage in our situation (see reference 42 for more specifics). The SMW formula is an expression for the inverse of the sum of an arbitrary nonsingular matrix $A$ and a matrix of small rank. Our Jacobian matrix can be written as the sum of a lower triangular matrix and a matrix, of much smaller rank, whose only nonzero entries are the upper right hand blocks of J. The SMW formula requires solving linear equations $Ay = \mathbf{b}$ for several different vectors $\mathbf{b}$ and is efficient when such systems are easy to solve, as is the case for our lower triangular matrix. For some parameter ranges this strategy was successful, and computationally fast. Unfortunately the procedure failed at small wave numbers. From our empirical experience, we place the blame for numerical instability in this situation on the lack of adequate pivoting; to preserve the lower triangular structure, pivoting was restricted to within the diagonal blocks (which is usually sufficient for a matrix arising from a discretized differential equations problem; see e.g., reference 27). To provide an alternative method without pivoting restrictions, we first dropped special treatment of the unknown parameter $\omega$ (or $k$) by writing a trivial differential equation for it:

$$\omega' = 0, \tag{A1}$$

(respectively, $k' = 0$). This trick (suggested to us by H. Keller) increases the number of differential equations by one but eliminates the left hand border of J. Next, since the

equations with periodic boundary conditions are equivalent to the same equations on a ring geometry, we renumbered the points on the ring as shown in Fig. A1 (suggested to us by C. Peskin). With this numbering, the blocks in the upper right hand corner of J are eliminated but at the cost of doubling the bandwidth of the matrix. With this formulation the Newton increment at each step is obtained by Gaussian elimination with partial pivoting for the band matrix without consideration for its block structure. This more adequate pivoting leads to no more than double the storage required by the band matrix itself. This procedure, for the third order backwards difference formula and points numbered as in Fig. A1, was more successful for small wave numbers.

The method described above may not be the most efficient method available for this problem. For example, in the case of small wave number, the increased storage requirement reduces the allowable number of mesh points and renders the desired accuracy unattainable. Subsequent to obtaining most of the results of this paper, additional calculations (particularly for small wave number) have been performed using the methodology and computer program developed by Pereyra (35). We presented the above description here for the purpose of acquainting the biophysically oriented reader with some of the computational subtleties of problems of this sort.

FOR SOLUTIONS OF THE CABLE EQ. 1 The authors used the well known Crank-Nicolson finite difference method (24) to compute the solutions to the cable equation presented in section 3. This method involves the solution of a set of nonlinear equations at each step. We can see this by writing the first part of Eq. 1 in the form:

$$V_t = \frac{a}{2RC} V_{xx} - I_i(V, m, h, n) \tag{A2}$$

Let $V_j^k$ be the value of the potential at time step $k$ and grid point $j$; $j = 0$ corresponds to $x = 0$. To solve the initial value problem for Eq. 1, we must have a way to find $V_j^{k+1}$ for all $j$, given values of $V_j^k$. The first thing we shall do is replace the second partial derivative with respect to $x$ in Eq. A2 by the centered difference approximation:

$$V_{xx,j}^k \approx (V_{j+1}^k - 2V_j^k + V_{j-1}^k)/(\Delta x)^2. \tag{A3}$$

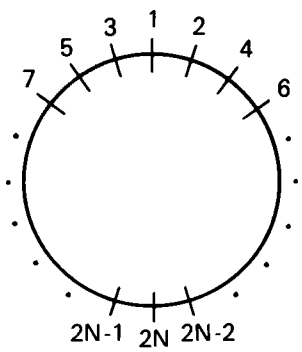


FIGURE A1 Numbering scheme for mesh points for ring geometry.

Here, $V^k_{xx,j}$ denotes the value of the second partial derivative of $V$ with respect to $x$ at the point $j$ at time $k$. Under this approximation, Eq. A2 becomes a set of simultaneous ordinary differential equations, each coupled to its immediate neighbors through the approximation Eq. A3. Explicit numerical methods of solving this set of ordinary differential equations are defined by the property that quantities of the form $V_j^{k+1}$ appear, in an uncoupled way, only on the left hand side of the equations. The simplest example of such a method is the forward Cauchy–Euler scheme:

$$(V_j^{k+1} - V_j^k)/(\Delta t) = \frac{a}{2RC}[V_{j+1}^k - 2V_j^k + V_{j-1}^k]/(\Delta x)^2 - I_i(V_j^k, m_j^k, L_j^k, n_j^k). \quad \text{(A4)}$$

Explicit schemes offer simplicity of computation at the cost of a restriction on the allowable time step $\Delta t$; implicit schemes can avoid this restriction at the cost of increased computational complexity. A discussion of the basic ideas of stability and accuracy of finite difference methods for partial differential equations can be found in Isaacson and Keller (24). A discussion of these considerations for the specific case of the cable Eq. 1 was given by Moore et al. (33). In our calculations we use the full Crank-Nicolson method:

$$(V_j^{k+1} - V_j^k)/(\Delta t) = \frac{a}{2RC} \cdot \frac{1}{2}[(V_{j+1}^{k+1} - 2V_j^{k+1} + V_{j-1}^{k+1}) + (V_{j+1}^k - 2V_j^k + V_{j-1}^k)]/(\Delta x^2)$$

$$- \frac{1}{2}[I_i(V_j^{k+1}, m_j^{k+1}, h_j^{k+1}, n_j^{k+1}) + I_i(V_j^k, m_j^k, h_j^k, n_j^k)], \quad \text{(A5)}$$

with $\Delta x = 0.05$ cm and $\Delta t = 0.01$ ms. This requires the solution of a system of nonlinear equations at each step. We solved these equations by the method of successive approximations. Our scheme differed little from that of Cooley and Dodge (7). Moore et al. (33), however, treat the nonlinear part of the system explicitly; that is, in Eq. A5 instead of the average of $I_i$ at times $k + 1$ and $k$, they use $I_i$ evaluated only at time $k$. This approach succeeds in removing the severe restriction on the time step, and involves the solution of a set of simultaneous linear equations, which can be done directly without an iterative scheme. Further, it is easier to program and cheaper to run. However, it is not as accurate as the scheme of Eq. A5; it will produce errors proportional to $\Delta t$, while the errors from scheme Eq. A5 will be proportional to $(\Delta t)^2$. Further, the stability properties may not be precisely the same as those of the Crank-Nicolson scheme because the nonlinear function $I_i$ in general has a linear part, and thus the linearized scheme is not identical to the standard Crank-Nicolson method for a diffusion problem. This partially explicit treatment was successful for Moore et al. (33), and may well provide sufficient accuracy and stability for a wide range of problems. Nevertheless, one should bear in mind the fact that the partially explicit treatment may not have all of the desired properties of Eq. A5 in a given problem.

Finally, we remark that for numerical accuracy the stimulus $I_s(t)$ was treated by incorporating it into Eq. 1 as a point source (see also reference 7). For this, we use the Dirac delta function $\delta(x)$ and add $I_s(t)\delta(x)/(2\pi a)$ to the right hand side of the first part of Eq. 1. Then, assuming even symmetry about $x = 0$, the difference equation for $j = 0$ is Eq. A5 with $V_{-1}^k$, $V_{-1}^{k+1}$ replaced by $V_1^k$, $V_1^{k+1}$, respectively, and with $(1/2\Delta x)\ (I_s^{k+1} + I_s^k)\ /\ (2\pi a)$ added to the right hand side.

The authors gratefully acknowledge the helpful comments and suggestions received during the course of this project from Prof. Charles S. Peskin of the Courant Institute of Mathematical Sciences, New York University, New York. J. Rinzel wishes to thank R. LeVeque for implementing a version of Pereyra's program PASVA3. The referees also offered valuable comments which we appreciate.

*Received for publication 23 May 1980 and in revised form 10 December 1980.*

## REFERENCES

1. Adelman, W. J., and R. FitzHugh. 1975. Solutions of the Hodgkin-Huxley equations modified for potassium accumulation in a periaxonal space. *Fed. Proc.* 34:1322–1329.
2. Arshavskii, Y. I., M. B. Berkinblit, and V. L. Dunin-Berkovskii. 1965. Propagation of pulses in a ring of excitable tissues. *Biophysics.* 10:1160–1166.
3. Bullock, T. H. 1951. Facilitation of conduction rate in nerve fibers. *J. Physiol. (Lond.).* 114:89–97.
4. Carpenter, G. A. 1977. Periodic solutions of nerve impulse equations. *J. Math. Anal. Appl.* 58:152–173.
5. Carpenter, G. A. 1979. Bursting phenomena in excitable membranes. *SIAM J. Appl. Math.* 36:334–372.
6. Casten, R., H. Cohen, and P. A. Lagerstrom. 1975. Perturbation analysis of an approximation to the Hodgkin-Huxley theory. *Quart. Appl. Math.* 23:365–402.
7. Cooley, J. W., and F. A. Dodge, Jr. 1966. Digital computer solutions for excitation and propagation of the nerve impulse. *Biophys. J.* 6:583–599.
8. Donati, F., and H. Kunov. 1976. A model for studying velocity variations in unmyelinated axons. *IEEE Trans. Biomed. Eng.* BME-23, No. 1. 23–28.
9. Evans, J. W., and J. Feroe. 1977. Local stability theory of the nerve impulse. *Math. Biosci.* 37:23–50.
10. Feroe, J. 1981. Existence and stability of multiple impulse solutions of a nerve conduction equation. *SIAM J. Appl. Math.* In press.
11. FitzHugh, R. 1969. Mathematical models of excitation and propagation in nerve. *In* Biomedical Engineering. H. P. Schwann, editor. McGraw-Hill Book Company, New York.
12. FitzHugh, R. 1973. Dimensional analysis of nerve models. *J. Theor. Biol.* 40:517–541.
13. FitzHugh, R., and H. A. Antosiewicz. 1959. Automatic computation of nerve excitation—detailed corrections and additions. *J. SIAM.* 7:447–457.
14. Gardner-Medwin, A. R. 1972. An extreme supernormal period in cerebellar parallel fibers. *J. Physiol. (Lond.).* 222:357–371.
15. Gear, C. W. 1971. Numerical Initial Value Problems in Ordinary Differential Equations. Prentice-Hall, Inc., Englewood Cliffs, N.J.
16. George, S. A. 1977. Changes in interspike interval during propagation: quantitative description. *Biol. Cybernetics* 26:209–213.
17. George, S. A., P. Rugg, and D. Mastronarde. 1976. Changes in interspike interval in fibers using a temporal sequence code. *Neurosci. Abstr.* 2:483.
18. George, S. A., and P. T. Silberstein. 1977. Conduction velocity after effects of spike activity: quantitative studies. *Neurosci. Abstr.* 3:677.
19. Hastings, S. P. 1976. The existence of homoclinic and periodic orbits for the FitzHugh-Naqumo equations. *Quart. J. Math. (Oxford).* 27:123–134.
20. Hodgkin, A. L., and A. F. Huxley. 1952. A quantitative description of membrane current and its application to conduction and excitation in nerve. *J. Physiol. (Lond.).* 117:500–544.
21. Householder, A. S. 1964. The Theory of Matrices in Numerical Analysis. Blaisdell Publishing Company, New York.
22. Huxley, A. F. 1959. Can a nerve propagate a subthreshold disturbance? *J. Physiol. (Lond.).* 148:80P–81P.
23. Huxley, A. F. 1959. Ionic movements during nerve activity. *Ann. N. Y. Acad. Sci.* 81:221–246.
24. Isaacson, E., and H. B. Keller. 1966. Analysis of Numerical Methods. John Wiley & Sons, Inc., New York.
25. Karfunkel, H. R., and C. Kahlert. 1977. Excitable chemical reaction systems. II. Several pulses on the ring fiber. *J. Math. Biol.* 4:183–185.
26. Keener, J. 1980. Waves in excitable media. *SIAM J. Appl. Math.* 39:528–548.
27. Keller, H. B. 1974. Accurate difference methods for nonlinear two point boundary value problems. *SIAM J. Numer. Anal.* 11:305–320.
28. Kocsis, J. D., H. A. Swadlow, S. G. Waxman, and M. H. Brill. 1979. Variation in conduction velocity during the

relative refractory and supernormal periods: a mechanism for impulse entrainment in central axons. *Exp. Neurol.* 65:230–236.
29. Maginu, K. 1978. Stability of periodic travelling wave solutions of a nerve conduction equation. *J. Math. Biol.* 6:49–57.
30. Mauro A., F. Conti, F. Dodge, and R. Schor. 1970. Subthreshold behavior and phenomenological impedance of the squid giant axon. *J. Gen. Physiol.* 55:497–523.
31. McKean, H. P. 1970. Nagumo's equation. *Adv. Math.* 4:209–223.
32. Miller, R. N. and J. Rinzel. 1978. Computation of periodic travelling wave solutions to the Hodgkin-Huxley equations. *Notices Amer. Math. Soc.* 25:1A–174A.
33. Moore, J. W., F. Ramon, and R. W. Joyner. 1975. Axon voltage clamp simulation. I. Methods and tests. *Biophys. J.* 15:11–24.
34. Nagumo, J., S. Arimoto, and S. Yoshizawa. 1964. An active pulse transmission line simulating nerve axon. *Proc. IEEE.* 50:2061–2070.
35. Pereyra, V. 1981. PASVA3: an adaptive finite difference FORTRAN program for first order nonlinear ordinary boundary problems. Proceedings of the Working Conference on Codes for Boundary Value Problems in ODE's. Houston, Texas, May 1978. Lecture Notes in Math. Springer Verlag, Berlin. In press.
36. Peskin, C. 1976. Partial Differential Equations in Biology. Courant Institute of Mathematical Sciences, New York.
37. Ramon, F., J. Vergara, and J. W. Moore. 1973. Changes in speed of propagation of action potentials in squid giant axons: experimental and computed results. *Biophys. J.* 13 (2, pt.2):131A. (Abstr.).
38. Raymond, S. A. 1977. Changes in conduction velocity accompany activity—dependent shifts in threshold of frog sciatic nerve. *Neorosci. Abstr.* 3:698.
39. Rinzel, J. 1975. Spatial stability of traveling wave solutions of a nerve conduction equation. *Biophys. J.* 15:975–988.
40. Rinzel, J. 1977. Repetitive nerve impulse propagation: numerical results and methods. *In* Nonlinear Diffusion, W. E. Fitzgibbon III and H. F. Walker, editors. Research Notes in Mathematics. Pitman, London.
41. Rinzel, J., and J. B. Keller. 1973. Traveling wave solutions of a nerve conduction equation. *Biophys. J.* 13:1313–1337.
42. Rinzel, J., and R. N. Miller. 1980. Numerical calculation of stable and unstable periodic solutions to be Hodgkin-Huxley equations. *Math. Biosci.* 49:27–59.
43. Rinzel J. 1980. Impulse propagation in excitable systems. *In* Dynamics and Modeling of Reactive Systems, Inc., W. E. Stewart, H. W. Ray, and C. C. Conley editors. Academic Press, Inc., New York.
44. Scott, A. C., and S. D. Luzader. 1979. Coupled solitary waves in neurophysics. *Physica Scripta.* 20:495–501.
45. Stein, R. B. 1967. The frequency of nerve action potentials generated by applied currents. *Proc. R. Soc. Lond. B. Biol. Sci.* 167:65–86.
46. Swadlow, H. A., and S. G. Waxman. 1975. Observations on impulse conduction along central axons. *Proc. Natl. Acad. Sci. U.S.A.* 75:5156–5159.
47. Swadlow, H. A., and S. G. Waxman. 1976. Variations in conduction velocity and excitability following single and multiple impulses of visual callosal axons in the rabbit. *Exp. Neurol.* 53:128–150.
48. Waxman, S. G., J. D. Kocis, and R. E. Foster. 1980. Impulse initiation in spinal neurons: cytochemical demarcation of the trigger zone, development of specialized axonal regions, and determinants of interspike intervals. *In* Abnormal Nerves and Muscles as Impulse Generators. W. Culp and J. Ochoa, editors. Oxford University Press, Oxford, England.